International Journal of Greenhouse Gas Control 153 (2026) 104660

Contents lists available at ScienceDirect

International Journal of Greenhouse Gas Control

journal homepage: www.elsevier.com/locate/ijggc

# A comparative multiscale analysis for $CO_2$ storage in giant saline aquifers inspired by the storage case of Santos Basin in Brazil

Mathias José Kreutz Erdtmann [a,b,*], Filipe Silva Lira [a,b], Sebastian Geiger [a], Hadi Hajibeygi [a]

[a] Faculty of Civil Engineering and Geosciences, Department of Geoscience and Engineering, Delft University of Technology, Stevinweg 1, 2628 CV, Delft, The Netherlands

[b] Petrobras - Petróleo Brasileiro S.A., Av. Republica do Chile, 65, Rio de Janeiro, Brazil

ARTICLE INFO

*Keywords:*
Underground carbon dioxide storage
Residual trapping
Multiscale simulation
Algebraic dynamic multilevel method
Multiphase flow
Porous media
Aquifers

ABSTRACT

Multiscale simulation frameworks are essential to quantify the $CO_2$ trapping and migration in large-scale saline aquifers, which entail highly-resolved fine-scale heterogeneous properties. However, classical upscaling approaches which aim to define effective properties on larger grid sizes can lead to significant and systematic overestimation of the solubility and residual trapping mechanisms. Reliable assessment of these two trapping mechanisms is crucial to ensure the integrity of the storage process and properly mitigate the leakage risks. Therefore, it is essential to develop advanced simulation technologies that are both accurate and efficient (i.e., scalable) for simulation of complex $CO_2$ plume dynamics within large-scale heterogeneous reservoir models. To overcome this challenge, in this work three advanced strategies are developed and investigated: Effective Values (EV) for parameters, Local Grid Refinement (LGR) and Algebraic Dynamic Multilevel (ADM). The numerical investigations specially include a set of consistent models in the Ponta Aguda saline aquifer, with a total area of 40,000 $km^2$, located offshore the Brazilian coast. The results indicate that the ADM is a promising method, delivering stable and robust results in a representative section of the field. This encourages further extensions of this method for real-field deployment. Specially, LGR and EV are found to be limited in their scopes for field simulations, since they depend on a matching pre-procedure (against a reference solution) for their upscaled parameters before any new simulations can be run. In addition, their tuned parameters cannot be transferred from one model to another. ADM, on the other hand, does not require any upscaling procedure, as the multiscale basis functions allow for consistent mapping across resolutions.

## 1. Introduction

Giant saline aquifers (defined here as aquifers with an area greater than 10,000 $km^2$) could be ideal candidates for $CO_2$ storage due to their significant storage capacity (Ringrose et al., 2021). However, for the same reason, accurate quantification of plume transport and migration, as well as reliable assessments of trapping and sealing mechanisms for these aquifers, are quite challenging (Celia et al., 2015; Mim et al., 2023). The reason is that reliable simulation of $CO_2$ migration and trapping in giant aquifers requires highly resolved grids (Lyu and Voskov, 2023; Ni et al., 2025), which are beyond the computational capacity of classical numerical schemes for simulations of such size. In addition, these aquifers often have significant uncertainties in their reservoir architecture, seal integrity, and associated petrophysical properties. As such, several simulations are required to quantify the ranges of capacity, injectivity, and safety level produced by this uncertainty, which will become better constrained once the operation starts, and the geological data are collected and incorporated in the forward simulations. This gives rise to the need for computationally efficient simulation techniques. Additionally, simulating the complex physics occurring during $CO_2$ injection into saline aquifers is challenging: the nonlinear and linear systems face convergence challenges, especially because capillary heterogeneity and relative permeability hysteresis are considered (Iglauer, 2011; Celia et al., 2015). An important factor is that oversimplifications, either through excessively upscaled models on very low resolution (coarse) grids or simplifying the physical processes such as neglecting hysteresis, can indeed lead to wrong estimation of the trapped $CO_2$ mass in the reservoir (Nordbotten et al., 2012, 2024; Wang et al., 2022). This imposes significant risks for a storage project. Therefore, developing a feasible computational framework that allows

* Corresponding author at: Faculty of Civil Engineering and Geosciences, Department of Geoscience and Engineering, Delft University of Technology, Stevinweg 1, 2628 CV, Delft, The Netherlands.

*E-mail addresses:* M.J.KreutzErdtmann@tudelft.nl (M.J. Kreutz Erdtmann), F.S.L.SilvaLira@tudelft.nl (F.S. Lira), S.Geiger@tudelft.nl (S. Geiger), H.Hajibeygi@tudelft.nl (H. Hajibeygi).

https://doi.org/10.1016/j.ijggc.2026.104660
Received 28 November 2025; Received in revised form 31 March 2026; Accepted 12 April 2026
Available online 17 April 2026

for efficient and accurate estimations of plume migration is essential, especially for large-scale aquifers. Note that the recent establishment of the simulation benchmark studies, specially the FluidFlower (Flemisch et al., 2024) and SPE11 (Nordbotten et al., 2025), are essential for validating the simulation approaches on lab-scale experiments, while benchmarking with field-data at in-situ conditions remains as an unresolved research challenge (Lopez-Saavedra et al., 2025; Misaghi Bonabi et al., 2025). These benchmarking studies have also highlighted the importance of grid resolution (Zhao et al., 2025; Hadjisotiriou et al., 2025; Kachuma et al., 2026) and challenges to speed up the simulations (Wang et al., 2024; Zhao et al., 2025; Pour et al., 2023), emphasizing the need of advanced simulation techniques.

As will be presented in this work, classical upscaling strategies to create coarse simulation models from relatively fine-scale geological models result in a significant and systematic overestimation of the trapped mass of $CO_2$, when compared to fully resolved reference simulations. These classical upscaling methods (based on geometric, arithmetic, or harmonic averaging and even flow-based methods) can account for the typical non-miscible multiphase flow, but may fail to consider the complex dynamics of highly reactive fluids such as $CO_2$. This is because classical upscaling approaches distribute phases on coarser grid cells, leading to lower saturation (volume fraction) values for the same mass (Pickup et al., 2010; Ukaegbu et al., 2009; Doughty and Pruess, 2003). As a result, these artificially lower saturation values can correspond to the immobile relative permeability value ranges, leading to wrong estimation of the trapped fluid (Durlofsky and Chen, 2012).

One can improve the transport (relative permeability and capillary pressure) functions at coarser grids considering the sub-grid heterogeneous properties (Pickup et al., 1994, 2010; Krevor et al., 2015; Wenck et al., 2024). However, applicability of this approach on giant aquifers, with highly heterogeneous coefficients may not be straightforward, and stays outside the scope of our simulation-focused article. Alternatively, vertical equilibrium (VE) models can be applied to reduce the simulation costs when the multiphase distribution across the vertical depth reaches an equilibrium (Court et al., 2012,?; Guo et al., 2014). The application of VE in thick, heterogeneous reservoirs with no real vertical depth equilibrium is not straightforward either. Nevertheless, since VE is applicable to provide a rapid first-order good estimates in regional scales, whenever the equilibrium assumptions hold, it can be indeed incorporated in field scale analyses to identify the sub-zones for more precise analyses (Doster et al., 2013; Buntic et al., 2025). Such extension can be incorporated in our workflow for future developments for relatively thin reservoirs (and not the currently focused giant fields with strong dynamics transport phenomena from near well-bore to the far field) (Bandilla et al., 2019; Alamara et al., 2025).

In addition to the incorrect estimations for relative permeability values, dissolution rates (which are enhanced by fingering effects or vertical migration) may also be unreliable in upscaled simulation techniques. Estimating solubility trapping is key to assessing long-term storage security during CCS (Benson et al., 2005; Zhang et al., 2017, 2025). Coarse grids can lead to suppression the fingering effects and excessive numerical (nonphysical) diffusion rates, further increasing the errors in simulation results of $CO_2$ trapping and storage security (Pau et al., 2010). In general, the loss of detail ultimately produces an oversimplification of reservoir heterogeneities and their effects on flow (Bentley and Stephens, 2026). Therefore, it is essential to develop multiscale simulation strategies that not only significantly reduce computational cost, but also result in reliable estimations of the distribution and trapped mass of $CO_2$ in giant heterogeneous aquifers.

Several multiscale strategies have been developed in the literature for multiphase flow in heterogeneous media (Durlofsky and Chen, 2012; Noetinger and Zargar, 2004). Here, we consider and compare three main approaches that have been extensively tested. However, they are not yet fully evaluated for $CO_2$ storage in giant aquifers. First, the Localized Grid Refinement (LGR) approach is used, which is a standard strategy to deal with complex systems on large-scale domains (Barbosa Machado et al., 2024; Syrakos et al., 2012). LGR has been extensively developed and applied to compute fluid flow in heterogeneous porous media (Michaud and Bisshopp, 1981; Dahle et al., 1992; Awid et al., 2018). Second, the Effective Value (EV) strategy is considered, which builds its coarse-scale grid properties by tuning against representative (reference) results (Durlofsky, 1991; King and Mansfield, 1999). Here we assume that the reference solution for which the parameters are tuned is given. This is a major challenge for using EV in real-field domains, for which reference representative solutions may not be available. Finally, we evaluate the Algebraic Dynamic Multilevel (ADM) modeling approach, which has been originally developed for multiphase immiscible systems (Cusini et al., 2016; HosseiniMehr et al., 2020). In this work, the extension of the ADM to account for complex thermodynamics and compositional effects (Zhao et al., 2025) was adapted and applied as a viable alternative to multiscale simulation in giant saline aquifers, covering the trapping mechanisms and the migration of the $CO_2$ plume in these aquifers. The classical upscaling approach (Christie and Blunt, 2001), including porosity averaging and flow-based permeability upscaling, is also considered to demonstrate its limitation when applied to the new context of $CO_2$ storage.

The three multiscale strategies, as well as the classical upscaling approach, are applied to a heterogeneous giant aquifer, inspired by the Santos basin in Brazil (Lira et al., 2025). Based on the results, both ADM and EV are found to be effective because they provide trapping estimates, including solubility and residual trapping, that are consistent with that of the reference solution. However, EV depends on a parameter-tuning step that can only be reliably performed if representative high-resolution reference solutions exist. In real-field applications, finding a reference solution to tune parameters can be challenging. These constraints limit the feasibility of the EV approach for real cases. Overall, it is found that ADM is in fact a promising method for simulations of $CO_2$-brine multiphase flow in giant aquifers.

Typically, different objectives are often pursued at different scales, from near well-bore to the giant real field. For example, the regional evaluation of the pressure interactions between multiple injection sites can be done via a hierarchical approach (Tveit et al., 2025).

In addition to the comparative analyses between different simulation strategies, to the best of our knowledge, this study is the first of its kind which considers 3D simulations for giant aquifers, with the focus on the field in Santos Basin that spans an area of 40,000 $km^2$, with a consistent novel multiscale framework. More precisely, to ensure that the full set of models actually represents the same storage complex, a robust multiscale framework must be devised. Such a framework is responsible for properly coupling multiple scales in terms of boundary conditions and upscaling methods, including consistency checks for both pressure and transport solutions. This novel framework produces a reliable and feasible method to simulate realistic storage projects in giant aquifers. More specifically, global-scale solutions allow for realization of the main driving forces and identification of the main fluid and pressure pathways, while local ADM-based simulations allow for detailed understanding of the extent of the $CO_2$ plume including the amount and local variation of trapped $CO_2$.

This manuscript is structured as follows: In Section 2, the governing equations are presented for modeling the porous media process, and Section 3 explores the methodology for multiscale and effective simulation strategies. Section 4 is dedicated to the description of the test case, including the definition of the parameters. The results and discussion are presented in Section 5. Finally, Section 6 presents the final remarks.

## 2. Governing equations

We assume that $CO_2$ storage in saline aquifers can be modeled as compressible two-phase flow in porous media while considering the three main trapping mechanisms (structural/stratigraphic, solubility,

and residual trapping). Hence, mass conservation for a multiphase multi-component $CO_2$-brine system can be stated as

$$\sum_{\alpha=w,n}\left[\frac{\partial}{\partial t}\left(\phi S_\alpha \rho_\alpha x_{c,\alpha}\right)+\nabla\cdot\left(\mathbf{u}_\alpha \rho_\alpha x_{c,\alpha}\right)-q_\alpha x_{c,\alpha}\right]=0, \tag{1}$$

where $\alpha$ denotes the phase, which is either the aqueous (or wetting phase) or supercritical $CO_2$ (or non-wetting phase). The terms "w" and "n" denote the wetting and nonwetting, respectively, and $c$ denotes the components ($CO_2$ and brine). Moreover, $\phi$ is the porosity of the medium, $s_\alpha$, $\rho_\alpha$, and $q_\alpha$ are saturation, density, and source term of phase $\alpha$, respectively. The phase velocity is $\mathbf{u}_\alpha$, and $x_{c,\alpha}$ is the mass fraction of component $c$ in phase $\alpha$. Darcy's law is employed to relate the phase velocity and pressure gradient, i.e.,

$$\mathbf{u}_\alpha=-\frac{k_{r,\alpha}\mathbf{k}}{\mu_\alpha}\left(\nabla p_\alpha-\rho_\alpha \mathbf{g}\right). \tag{2}$$

Here $\mathbf{k}$, $\mu_\alpha$, and $p_\alpha$ are the rock permeability, phase viscosity, and phase thermodynamic pressure. Moreover, $k_{r,\alpha}$ is the phase relative permeability. Phase pressures are related by capillary pressure, i.e., $p_{cap}=p_n-p_w$.

To solve Eqs. (1) and (2), we use the two-point flux approximation (TPFA) with fully implicit time discretization including a Newton–Raphson linearization. The pressure for the aqueous phase and the $CO_2$ total mole fraction are defined as primary variables, over all phase states.

For the solubility trapping and the definition of $CO_2$ distribution in aqueous phase, $CO_2$ solubility in brine is derived from k-values, which are provided as a function of pressure, temperature and salinity, calculated from Henry's law (Duan and Sun, 2003; Li and Nghiem, 1986; Sun et al., 2021). The Henry constant $H$ is related to the k-value $k_s$ as $H=k_s\cdot f p_w$ (where $f$ is the fugacity coefficient of $CO_2$ in the brine). This approach allows us to model the solubility gradient in thick reservoirs (Addassi et al., 2022; Zhao et al., 2025).

Residual trapping is caused by the hysteretic behavior of $CO_2$ in the presence of brine in a saline aquifer and is synergic with the structural trapping and smaller scale heterogeneities (Juanes et al., 2006; Zhang et al., 2025). In this work, the Land hysteresis model (Land, 1968) is employed, as it is widely used in the literature (Juanes et al., 2006; Ruprecht et al., 2014; AL homoud et al., 2024). Key to this model is the Land trapping coefficient $C$, which quantifies the relation between the initial saturation $S_{\alpha i}$ and the residual saturation $S_{\alpha r}$ after a drainage-imbibition cycle, i.e.,

$$S_{\alpha r}=\frac{S_{\alpha i}}{1+C\cdot S_{\alpha i}}.$$

Simulations of $CO_2$ injection for storage in brine using this set of governing equations are performed by two simulators: CMG-GEM software, version 2024.10 (Computer Modelling Group Ltd., 2024) on a 64-node computational cluster and DARSim (Delft Advanced Reservoir Simulator (DARSIM), 2024; Hajibeygi et al., 2020) on an 8-core workstation. The application of DARSim allowed the evaluation of one additional strategy for effective simulation at larger scales, as it is capable of applying adaptive multilevel grid. The solubility and residual trapping by hysteresis are modeled on the same principles in both simulators, and they were benchmarked to each other, providing equivalent results when all the parameters are equal. The Peaceman well-model formulation (Peaceman, 1983) with pressure-controlled constraint is used for the CMG-GEM simulations and equivalent volume controlled injection was used in DARSim (as a percentage of porous volume).

From these simulations, the contribution of the trapping mechanisms can be quantified. After 40 years of injection period, another 40 years are observed to evaluate the trapping mechanisms during $CO_2$ post-injection migration. Fig. 1 shows a representative cross-section of the typical setting for the $CO_2$ storage test used in this study. These periods were selected to highlight the most critical time frame for projects from an operator perspective. The injection and early post-injection period needs increased attention, as it is the time interval in which most of the monitoring and regulatory commitments are made.

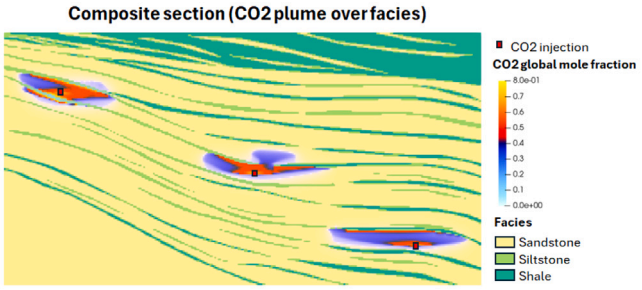


**Fig. 1.** Representative cross-section of a fluvio-deltaic system where $CO_2$ injection is simulated using DARSim for a period of 80 years, composed by 40 years of injection and 40 years of post-injection migration.

A complementary study of long-term post injection is beyond the scope of this comparative study, although it can be relevant for storage performance analyses in general. Specially, long-term highly-detailed analysis, as presented in this work, for the time period of 80 years requires a multiscale strategy in time, which is beyond the scope of this study. For reference, notice that the most computationally expensive fine scale simulations presented in this work required nearly 18 days to run with using a HPC cluster.

Geomechanical processes were not modeled. However, injection pressure and rates were constrained so that the reservoir pressure remain below 90% of the minimum stress gradient (estimated as 14.5 kPa/m from regional data for the basin in which the test case is located), reducing the likelihood of geomechanical processes (such as unintentional hydraulic fracturing) influencing storage operations.

## 3. Methodology

This is a comparative study that aims to evaluate the accuracy of different strategies to model trapping mechanisms reliably in large-scale reservoir settings. The strategies evaluated are: Local Grid Refinement (LGR), Effective Values (EV) and Algebraic Dynamic Multilevel (ADM). To add further value to this analysis, we consider a real-world case study: a giant aquifer called Ponta Aguda, that is located in the Santos basin (Brazil), near emission centers, as illustrated by Fig. 2. It is a single hydraulic unit with area about 40,000 $km^2$ (100 km × 400 km) and up to 2000 m thick. The dimensions of the aquifer emphasize the need to reliably represent the trapping mechanisms across scales from tens of meters to hundreds of kilometers. The summary of the geological and flow modeling will be presented in the following sections.

### 3.1. Multiscale modeling

The proposed framework is illustrated in Fig. 3. This approach aims to enable the evaluation of giant aquifers with 3D flow simulations based on a set of consistent static and dynamic reservoir models, which make use of available data across different scales.

The multiscale models (Table 1) deliver results that are produced from geological modeling spanning on a range from tens of meters to hundreds of kilometers, so it is possible to simulate CO2 migration in the near-wellbore region to regional-scale pressure dissipation. The injection parameters (e.g., well location, injection pressure and rates) are defined accordingly for each scale (i.e. a single well for S1, a cluster of twelve wells for S2, multiple clusters for S3 and S4). This approach allows us to generate consistent simulation results for each scale and transfer key parameters between models. For example, the average pressure change within a control volume is the same from the largest scale to the smaller scale.

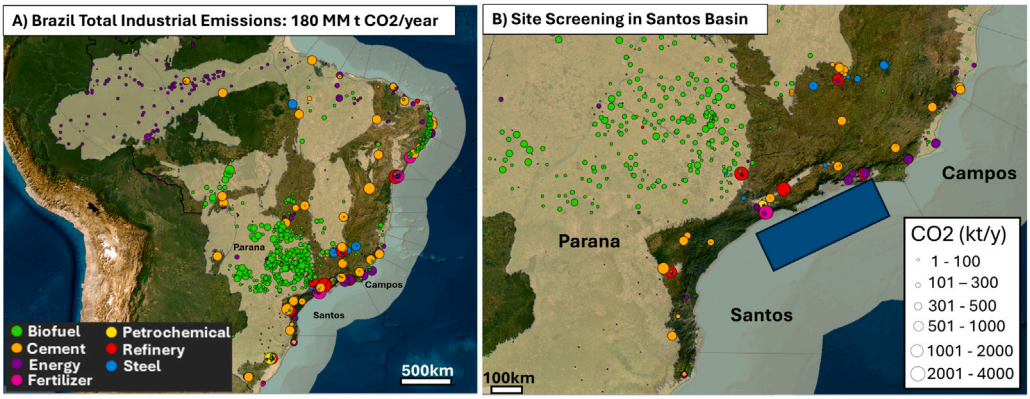


**Fig. 2.** Major sedimentary basins in Brazil with bubble map showing large-scale $CO_2$ emissions (left). Zoom-in of the Santos basin with the Ponta Aguda aquifer (right). Edited from Instituto do Petróleo e dos Recursos Naturais (I.P.R. - PUCRS) (2025)).

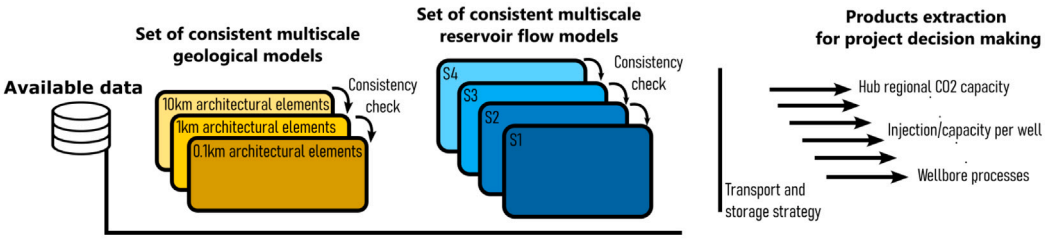


**Fig. 3.** Framework for multiscale modeling of large aquifers for $CO_2$ storage.

**Table 1**
Definition of scales and key outputs for large-scale aquifer modeling of CCS, using the Ponta Aquda saline aquifer as a test case. Each scale produces different outputs that provide important information that is needed for the storage design and analysis.

| Scale | Area covered | Domain | Output |
|---|---|---|---|
| S4 | $\times 10^4$ km$^2$ | Basin scale (40,000 km$^2$) | Required area for a regional storage hub (at least 1 Gt $CO_2$ capacity) |
| | | | General pressure effects over large areas |
| S3 | $\times 10^3$ km$^2$ | Hub scale | Expected capacity of a hub |
| | | (4250 km$^2$) | Relative capacity comparison between different cluster localization targets. |
| S2 | $\times 10^2$ km$^2$ | Cluster (Project) scale | Spatio-temporal plume evolution (saturation and pressure) for a project cluster. |
| | | (400 km$^2$) | Total injection rates/cumulative mass and injectivity variability between wells. |
| S1 | $\times 10^1$ km$^2$ | Single well neighborhood | Single well plume extension including possible faults |
| | | (16 km$^2$) | Vertical pressure gradient during injection to consider geomechanical constraints |

The different scales are named according to the order of magnitude of the area that they cover (Table 1). Each scale can be applied to evaluate specific aspects of the CCS operation that occur in the respective area.

Based on the available data, we created confidence maps to identify regions that provide better quality and quantity of information. Based on these maps, we then select the areas for which the models are built on different scales (Table 1).

Fig. 4 presents confidence maps for Ponta Aguda saline aquifer, with confidence scores based on the quality of the available well and seismic data. For the seismic confidence map, areas with sparse 2D lines (more than 2 km between lines) receive a score of 1, dense 2D lines a score 2, and full 3D coverage a score of 3. For the well density confidence map, a score of 1 was assigned to a density of up to 0.5 wells/100 km$^2$, a score of 2 for 0.5 to 5.0 wells/100 km$^2$ and a score of 3 for more than 5.0 wells/100 km$^2$. The joint score is then produced by summing seismic and well density scores. Areas with better data quality are associated with higher scores, and these are selected for smaller scales, requiring detailed models.

The dimensions of the model cells for each scale were chosen such that the models have between 5 and 15 million active grid cells, leading to cells with horizontal sizes of 33, 100, 250 and 1000 m for S1, S2, S3 and S4, respectively. The average grid thickness is 1, 3, 6 and 20 m (from S1 to S4). The construction of the geological elements for each scale is illustrated in Fig. 5. Geological modeling was performed for every scale, detailing architectural elements of 10 km on the larger scale (S4) and 1 km on the smaller scales (S3,S2). A more detailed geological, with 0.1 km architectural elements, improves the representation of the well scale (S1).

Each architectural element is a modeling element, defining a 3D rock body that is clearly distinct from one another. Its size is analogous to the reach of a variogram, but element-based, including geometrical distinctions, for example, of a deltaic front or a channel (Ringrose and Bentley, 2021). These elements are not necessarily homogeneous, and might have interval variability of porosity and permeability, as dictated

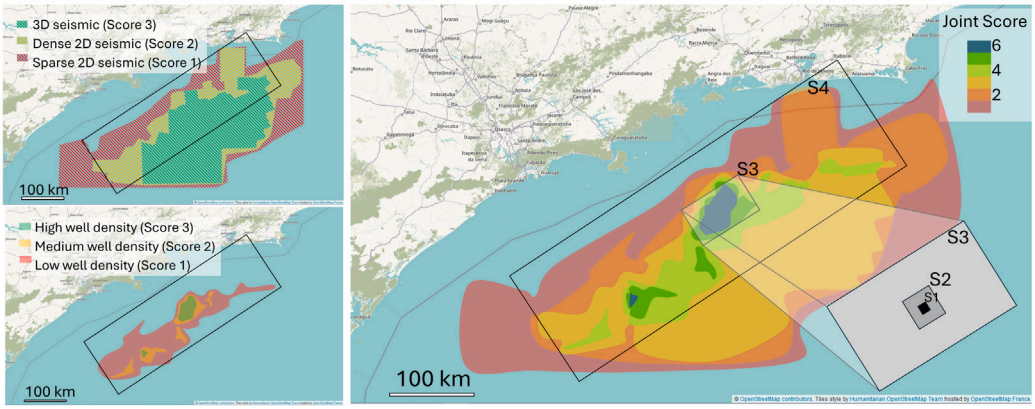


**Fig. 4.** Data confidence maps: seismic quality score (top left) and well density map (bottom left). These two maps are combined into a joint score map, showing the area with the most reliable data to build detailed models for smaller scales. The smaller scales overlap the region of larger scales.

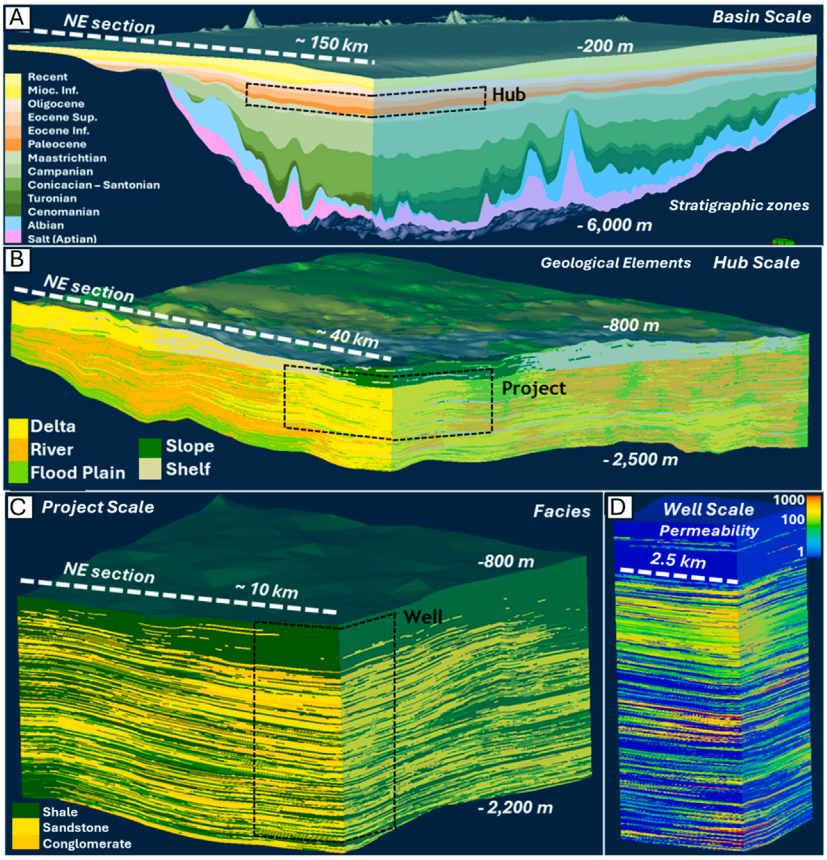


**Fig. 5.** Geological modeling for each scale from the scale with hundreds of kilometers (A) to the scale of few kilometers (D). In (A), the stratigraphic layering is presented, while in (B) the geological elements associated with the deposition environments are defined (deltaic, river, etc.), in the scale of tens of kilometers. In (C) the facies distribution provides a vision of the heterogeneity while in (D) a close-up of the permeability can be seen as the final product of the distributions.

by its conceptual model. Due to this internal variability, grid cells of a tenth of the element size provide a reasonable representation.

### 3.2. Consistency check by loosely coupled solution for multiscale simulation

When simulating a set of models constructed at different scales, it is important that at some point the results between scales must be checked for consistency. The average values for the pressure, saturation, soluble, and immobile $CO_2$ fractions computed using different scales must remain within an acceptable range. The saturation distribution operates on a local scale, while the pressure distribution operates on a regional scale, so the information from both simulated scales are connected (Hajibeygi et al., 2008).

This connection is achieved by defining boundary conditions to model pressure dissipation at smaller scales (from S1 to S3) according to pressure dissipation observed on larger scales (from S2 to S4, respectively). As long as the injected fluids are contained inside the limits of the model, its boundary conditions can be defined, allowing water to flow across the boundaries such that the average pressure matches

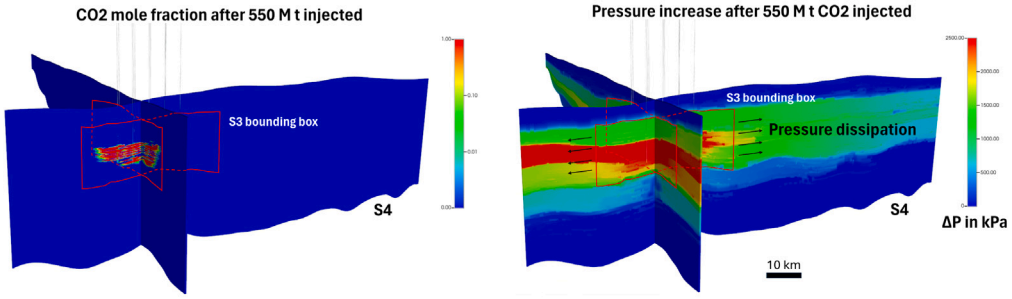


**Fig. 6.** Saturation and pressure distribution for the S4 scale model, i.e. the hub-scale. All saturation changes occur within the limits of S3, while pressure changes dissipate outside S3 limits. Vertical scale with 10:1 exaggeration.

the larger-scale model. This consistency check step is a loosely coupled solution, as the average pressure is matched, but not the whole pressure distribution (Hajibeygi et al., 2011). Fig. 6 shows the saturation and pressure distributions for model scales S3 and S4 (Table 1).

This loose coupling is achieved using the Fetkovich boundary formulation (Fetkovich, 1971), which provides the ability to parameterize the speed and magnitude of pressure dissipation from the lateral extents of the smaller to the larger scale models using productivity $J_w$ and volume $V_{out}$.

In the Fetkovich model, the flow rate $q_{out}$ from the outer volume (i.e., volume modeled by the larger scale) to the inner volume of the reservoir (i.e., volume modeled by the smaller scale) is defined as

$$q_{out} = J_w(p_{w,out} - p_{w,in}),$$

which is a function of the productivity index $J_w$, its current pressure $p_{w,out}$, and the reservoir pressure $p_{w,in}$.

In carbon storage scenarios, an overall pressure increase is expected, so the pressure in the inner volume is higher than the outer volume pressure and $q_{out}$ is negative (indicating the flow to the outer volume, leading to pressure dissipation).

The aquifer pressure is updated from the initial pressure $p_{w,i}$ proportionally to the cumulative influx $W_{out} = \int q_{out} dt$, assuming constant compressibility. Since $q_{out}$ is negative and assuming constant compressibility $c_t$, pressure dissipation will lead to an increase in the pressure of the outer volume, given by

$$p_{w,out} = p_{w,i} - \frac{1}{V_{out} \cdot c_t} \cdot W_{out}.$$

The total flow rate is then distributed to the boundary grid cells proportionally to the permeability of each connected cell.

The pressure consistency check must be performed from the largest scale to the smallest scale. After the boundary conditions are defined, the average pressure change is expected to remain similar (for the same control volume and injected $CO_2$ mass). An example of this consistency check is presented in Fig. 7. The Fetkovich boundary condition on the smaller scale (S3) allowed some of the total pressure to dissipate, and the pressure increase turned out to be smaller than that which was calculated with sealing boundaries, corresponding to the actual pressure changes in time of the large-scale solution (S4). This process is repeated for all scales, from S4 to S1.

### 3.3. Strategies for effective simulation at larger scales

As the size of the model increases from S1 to S4 (Fig. 5), the number of grid cells becomes intractable if the grid size stays as small as for the S1 system (i.e., well-scale). As such, there should be coarser grid sizes as the dimensions increase. This can only be achieved reliably if upscaled properties are defined on coarser grids. Reliable upscaling methods aim to reduce the number of grid cells (i.e., apply coarser grids) while ensuring that simulation results remain representative (Farmer, 2002). However, traditional upscaling methods, either by analytical or flow-based numerical methods, are only applicable for maintaining the quality of some properties such as porosity, (relative) permeability, and facies type (or mineralogy) (Durlofsky, 2005; Barker and Dupouy, 1999; Rabinovich et al., 2015; Wenck et al., 2024). Applying such upscaling methods to complex $CO_2$ systems where hysteresis and dissolution effects must be rigorously considered remains a challenge.

To resolve the limitation of globally applied upscaling methods, the Local Grid Refinement (LGR) method was developed by Dahle et al. (1992) and Syrakos et al. (2012) (See Fig. 8). LGR refines the grid in regions where steep gradients in petrophysical properties or solution variables prevail (e.g. the near-wellbore region, near saturation fronts, or in the vicinity of faults). Note that the rest of the domain (outside of the refined region) remains at a coarser grid resolution with upscaled parameters to improved computational efficiency without creating systematic errors in the simulation results (Syrakos et al., 2012). Since solution variables vary gradually in these regions, relatively coarse grid resolutions are sufficient.

The Effective Value (EV) method, as illustrated in Fig. 8, expands the idea of effective properties used in the upscaled model by allowing the tuning of dynamic parameters for solubility and residual trapping, similar to generating pseudo-curves when upscaling relative permeability and capillary pressure parameters (Rabinovich et al., 2015). During the tuning of the solubility and Land's hysteresis parameters, there could be a deviation from laboratory measurements, as observed with the generation of pseudocurves for relative permeability and capillary pressure upscaling (Rabinovich et al., 2015). On this proposed method, the effective solubility parameter (i.e. k-value) is defined by using a single constant multiplier for all the values in the original (fine grid) k-value function, i.e.,

$$k_{s,EV}(T, P, Salinity) = \alpha \cdot k_s(T, P, Salinity),$$

where $\alpha$ is the multiplier that will be tuned to find the equivalent system, and $k_s(T, P, Salinity)$ is the original function of pressure, temperature and salinity. When $\alpha > 1.0$ (i.e. higher effective k-value), the solubility is reduced. The same idea applies to Land's $C$ parameter, with a single constant, $\beta$, defining the equivalent value as $C_{EV} = \beta \cdot C$. Using a $\beta > 1.0$ tuning parameter will reduce the capillary trapping.

The basic concept of the EV method is analogous to that of relative permeability upscaling, in the sense that it promotes changes in a modeling parameter, allowing it to diverge from the fine scale laboratory measurement. However, while relative permeability upscaling tunes the curve shapes and the end points, the EV presented here adjusts the values of $\alpha$ and $\beta$ for solubility and residual saturation, respectively. This allows the method to directly capture the trapping mechanisms.

Finally, as shown in Fig. 9, Algebraic Dynamic Multilevel (ADM) retains the original fine-scale distribution of all properties, without using effective parameters, while dynamically applying a multi-level hierarchical simulation grid. The main idea behind ADM is to simulate flow and transport of components on the fine scale only near the (dynamic) fronts (i.e. where saturation of the injected fluid is larger

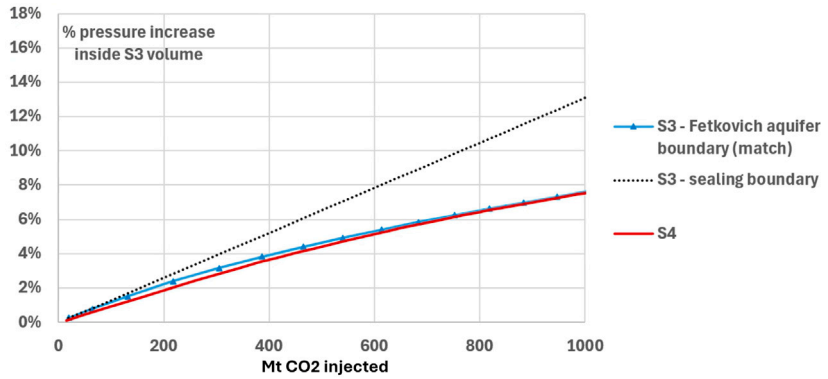


**Fig. 7.** Scale consistency check by adjusting pressure response with boundary condition. S4 covers 400 × 100 km (each cell has 1000 m horizontal size), while S3 covers 85 × 50 km (each cell has 250 m horizontal size).

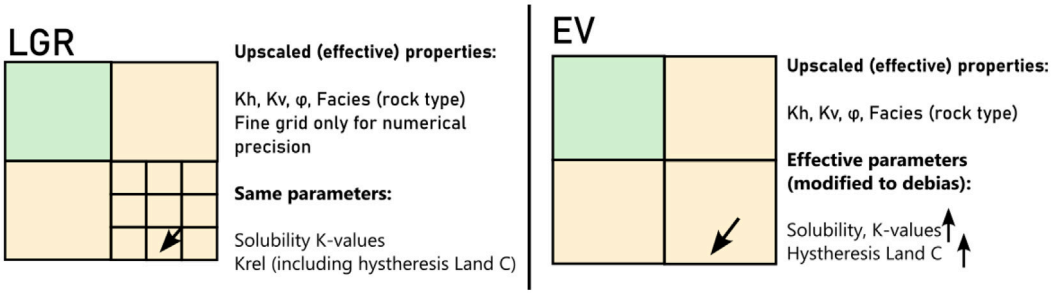


**Fig. 8.** LGR (left) introduces a refined grid in a selected area, but still uses the upscaled parameters. EV (right) has the same number of cells as an upscaled model, but allows tuning of dynamic parameters, such as solubility and hysteresis, in order to obtain good agreement between fine-scale and coarse-scale simulation models.

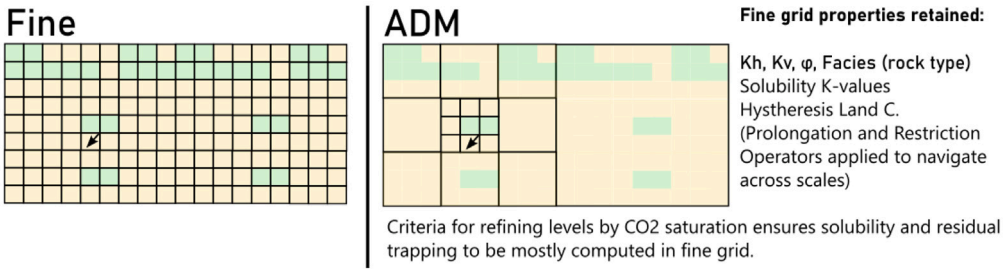


**Fig. 9.** Comparison of a fine-scale grid (left) and ADM (right). ADM is adaptive and dynamic, and thus changes the grid to allow fine grid computation of cells that have relevant changes in $CO_2$ saturation and concentration. The multi-level approach allows the grid to be coarsened and refined multiple times without compromising on solution accuracy.

than a defined threshold) and high-sensitive zones (e.g. near well-bores). As the rates of changes in saturation and pressure decreases in a given region, the dynamic multilevel gridding technique defines a coarse-scale grid resolution to improve computational efficiency without sacrificing solution accuracy (Hajibeygi et al., 2020; Hosseini-Mehr et al., 2020). Note that ADM does not depend on any upscaling parameter; instead it utilizes the multiscale basis functions to map between the coarser and finer scale pressure values (Hajibeygi et al., 2008), producing a dynamic grid, in contrast to the static grid applied in LGR.

More precisely, the transition between coarser and finer scales in ADM is obtained by using prolongation and restriction operators, constructed by basis functions, and can be made recursively, thus reaching a multilevel approach (Cusini et al., 2016). In this evaluation, two-level coarsening was allowed. ADM can be a powerful simulation approach because it does not require static upscaling or tuning of upscaled parameters; as long as a solution tolerance is defined, ADM can compute solubility and capillary trapping due to hysteresis on a coarse scale model at the same level of accuracy as a fine-scale model (Cusini et al., 2016; Hajibeygi et al., 2020; Zhao et al., 2025).

A detailed description of the construction of prolongation and restriction operators, as well as the definition of the basis functions for $CO_2$ storage in heterogeneous aquifers in ADM strategy, can be found in Zhao et al. (2025). Here we applied the same definitions that were tested specially against the SPE11 test case, using the DARSim version from this source (Zhao et al., 2025).

## 4. Case study: The giant ponta aguda aquifer, offshore Brazil

The potential of CCS in offshore aquifers in Latin America has previously been underestimated (Dunk et al., 2008), especially for Brazil, where the capacity for offshore $CO_2$ storage is at least 6 Gt even when only considering two (i.e., Paraná and Espirito Santo) of the five major basins (Campos, Santos, and São Francisco) that are located near major industrialized areas (Amarante et al., 2024).

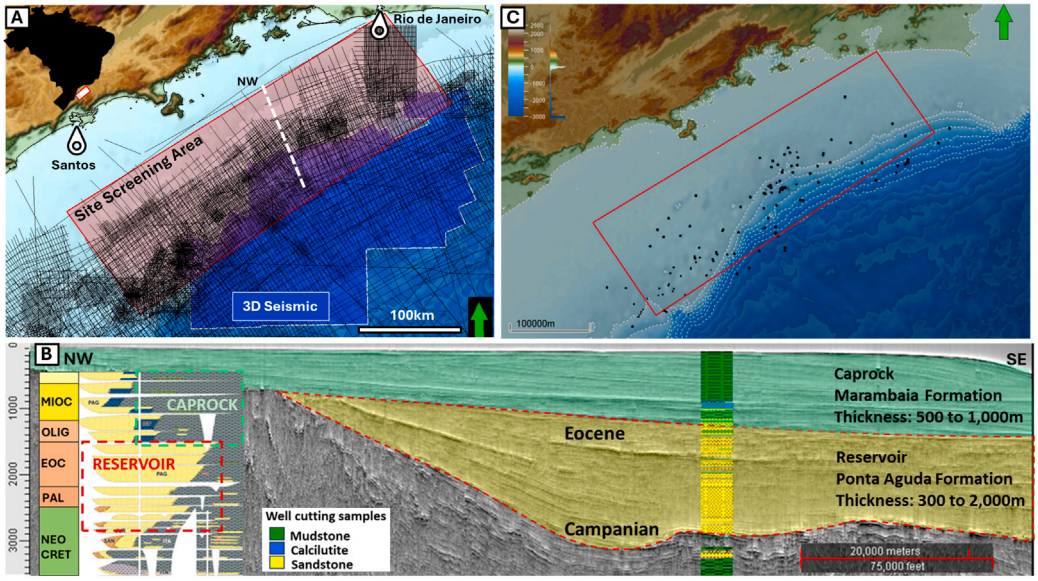


**Fig. 10.** Overview of the Ponta Aguda localization, edited from Lira et al. (2025). Location of the aquifer and the available seismic data (A). Stratigraphic section (B), and a detailed view of drilled wells (black dots) and selected study area (C).

The Paraná basin was subject to some evaluation efforts (Miotliński and Peeters, 2021), being a very sensitive area due to the existence of the regional Guarani freshwater aquifer (de Oliveira et al., 2023). Utilizing the saline aquifers in the offshore Santos and Campos basins allows a faster deployment of gigascale $CO_2$ storage in Brazil (Rockett et al., 2010).

The Santos and Campos sedimentary basins, despite 50 years of hydrocarbon exploration and production, still have knowledge gaps related to the extent, heterogeneity, and geological architecture of the underlying aquifers. One step in building confidence in offshore CCS in Brazil is to quantify the impact of these gaps on the storage volume, rates and integrity of a storage unit.

These two basins are located near major stationary $CO_2$ sources whose emissions amount to 117 Mt per year (Rockett et al., 2010). The existence of massive saline aquifers in the shallow waters of these basins is known since oil and gas exploration began in the 1970s and 1980s. The initial hypothesis of the oil and gas exploration effort was to repeat the success of the discoveries of oil and gas reservoirs in the Mississippi and Niger deltas, only to find that the sand content was too high on the Brazilian shelf, requiring wells to be drilled in deep waters before actually finding relevant oil and gas accumulations (Bacoccoli et al., 1979; Anjos et al., 2024).

What was, from an oil and gas perspective, for the last decades an inconvenient massive body of sand saturated only by water, can now be reevaluated as saline aquifers that are ideal candidates for carbon storage. The location of one of these relevant aquifers, named Ponta Aguda in the Santos basin, is presented in Fig. 10. The Ponta Aguda aquifer is a single hydraulic unit with an extension of 400 $x$ 100 km, a thickness of up to 2000 m, and a net-to-gross ratio of around 70% (Lira et al., 2025).

Fig. 10 also shows a representative cross section which follows a 2D seismic line that crosses one well. It is possible to observe the typical geology of the thick top shale over an extended interval of intercalated sandstone and shale layers with high overall sand content. The aquifer pinches out in the shallower, northwest portion and increased shale contents to the deeper portion. The presence of a top shale interval with a minimum thickness 500 m, can provide a final barrier to $CO_2$ migration.

The Ponta Aguda aquifer of the Santos basin is selected for the assessment of a carbon storage prospect and is hence an excellent real-world test case for a framework that aims to model CCS in large-scale regional aquifers.

The total area of the aquifer is approximately 40,000 km$^2$. Within this area, a 400 km$^2$ localized acreage must be characterized in detail. This smaller area is a prospect for a cluster of wells that are set to receive 5% of the regional emissions (6 Mt/year, or 240 Mt in 40 years). This would be a first phase of CCS development that is being considered as a possibility of development by Petrobras as a storage site for Rio de Janeiro or São Paulo $CO_2$ capture hubs. This development should occur in the S2 area of 400 km$^2$. There would be an option to scale up the project to store 25% of the emissions (30 Mt/year, or 1.2 Gt in 40 years) by expanding the injection to a storage hub with an area of 4000 km$^2$.

Producing static and dynamic engineering models for such a large area, including modeling the dynamics of $CO_2$ storage processes, is challenging. As discussed above, a multi-scale approach is needed to model and understand the overall behavior of the entire aquifer, while detailed observations of the plume migration must be generated at the project scale and around the wells. Thus, it is necessary to produce results that are consistent on a regional and localized scale.

### 4.1. Available data

159 wells were drilled through the Ponta Aguda aquifer. However, key parameters, such as permeability, relative permeability, and salinity, were not measured because the aquifer was not of economic interest. The available data comprises dense 2D seismic lines, 3D seismic cubes covering 30% of the area, logs for 156 wells (in general simplified logs combining density/neutron and resistivity), 30 m of core analysis, and pressure and temperature gradients measured in 22 wells on the deepest intervals. Table 2 provides a descriptive summary of the available data.

The lack of injectivity information for the aquifer is notable, as well as the lack of complete 3D seismic coverage. These data gaps give rise to uncertainties, notably reservoir connectivity and geomechanical limits, which must be evaluated and quantified. The same applies to other properties, such as salinity (which affects $CO_2$ solubility), relative permeability, and capillary pressure, which directly impact trapping mechanisms.

### 4.2. Model parameterization and test cases

A summary of the five different model parameterizations is presented in Table 3. The dimensions of the cells in the DARSim simulations are the same as those in the S2 scale (CMG-GEM simulator), and the $CO_2$ injection reproduces the same percentage of pore volume.

**Table 2**
Data available for the Ponta Aguda aquifer.

| Data | Availability | Comments |
|---|---|---|
| Seismic | 2D and 3D | 3D covering 30% of the occurrence area, fair density of 2D coverage overall |
| Well logs | 156 wells | Mixed quality, including cuttings description and electrical logs |
| Core analysis | 30 m | Representative of lower interval inside Ponta Aguda aquifer, lacks upper interval porosity and permeability data |
| Brine composition | No data | Using regional data |
| Temperature/pressure gradient | 22 wells | Representative of lower interval |
| Salinity gradient | No direct sample | Defined consistently with pressure gradient, affects solubility gradient |
| Relative Permeability/Capillary pressure/Hysteresis | No sample | Assuming typical values per facies for fluvial sands |
| Geomechanical properties | No sample | Assumed regional properties |
| Fracture effects/pressure diffusivity | No dynamic data | Assumed fracture and mobility behaviors. Assumed dynamic injectivity from inferred permeability distribution. |

**Table 3**
Simulation parameters for different models used in this study.

| | S1 | S2 | S3 | S4 | Representative 2D section | Homogeneous 2D section |
|---|---|---|---|---|---|---|
| $\phi$ (average) | 16.4% | 16.1% | 15.2% | 13.6% | 16.0% | 16.0% |
| $k$ (log-average [mD]) | 28 | 30 | 21 | 18 | 30 | 30 |
| $k_v/k_h$ | 0.1 | 0.1 | 0.1 | 0.1 | 0.1 | 0.1 |
| Lorenz Coefficient (for a well in the central location) | 0.77 | 0.77 | 0.7 | 0.6 | 0.7 | 0 |
| % shale/silt | 35% | 35% | 40% | 44% | 26% | 0% |
| Cell horizontal size [m] | 33 | 100 | 250 | 1000 | 100 | 100 |
| Cell vertical size [m] | 1 | 3 | 6 | 20 | 3 | 3 |
| Numerical aquifer pore volume [G $m^3$] | 2.2 | 62 | 460 | 5400 | 0.16 | 0.21 |
| Injected mass [Mt] | 30 | 293 | 2320 | 2320 | 0.74 | 0.95 |
| Injected pore volumes | 1.9% | 0.6% | 0.7% | 0.1% | 0.6% | 0.6% |
| Well count | 1 | 12 | 96 | 96 | 3 | 3 |
| Simulator | CMG-GEM | CMG-GEM | CMG-GEM | CMG-GEM | DARSim | DARSim |
| Cell count | 6 M | 11 M | 8 M | 15 M | 44 k (2D) | 44 k (2D) |
| Grid geometry | Corner point | Corner point | Corner point | Corner point | Cartesian | Cartesian |

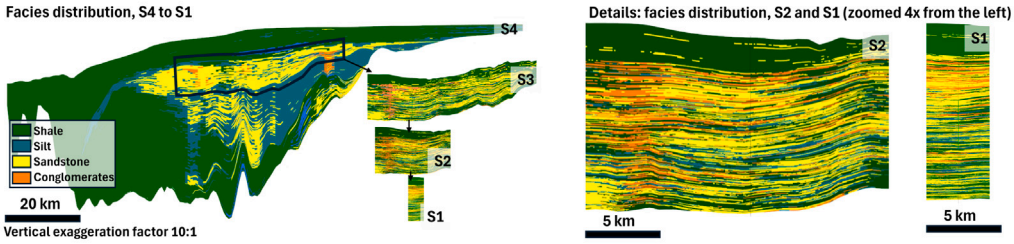


**Fig. 11.** Geological models with increasing facies detail at smaller scales. Note the lack of resolution in the facies scales for the larger models, especially S4.

Beyond the average values for the parameters, the heterogeneity (quantified by the Lorenz Coefficient (Shook and Mitchell, 2009)) of the reservoir is key to determine the spatio-temporal evolution of the $CO_2$ plume during injection, providing a synergy between structural/stratigraphic trapping and residual/solubility trapping (Zhang et al., 2025).

The geometry of the corner-point grid is generated by the interpreted surfaces from the seismic images and drilled wells' markers. Despite the existence of erosion events, they are not extreme and are configured by juxtaposition of sand-rich intervals. The facies distribution (distinguishing between shale, fine, medium and coarse sands) was generated for each model based on the distribution of the wells and the conceptual depositional model as illustrated by Fig. 11. From the facies, the porosity and permeability distributions were derived (Lira et al., 2025).

The rock-fluid characterization included the petrophysical properties of the fine sand facies (composed of shale and siltstone), which eventually allowed $CO_2$ flow to occur in the low-permeability layers. Due to the lack of specific laboratory data for the Ponta Aguda aquifer, the relative permeability curves were defined according to the literature and regional data (Burnside and Naylor, 2014; Alipour K. et al., 2022). Two sets of relative permeability curves are applied: one for fine facies (siltstone and shale) and another for sandstone, including capillary pressure curves and the Land hysteresis parameter of 1.0 for sandstone and 0.35 for shale and siltstones (Fig. 12). The average permeability for shale/silts is 0.1mD and for sandstones 30 mD (with a porosity around 16%).

The temperature and salinity gradients were defined based on data from 22 wells. The temperature varies from 40 to 70 °C from the top seal (1000 m depth) to the injection depth (2000 m). The salinity ranges from 80,000 to 130,000 g/l for the same depths. The salinity gradient is obtained indirectly by comparing the pressure measurements with the calculated hydrostatic gradient for the assumed salinity gradient. These gradients are presented in Fig. 13.

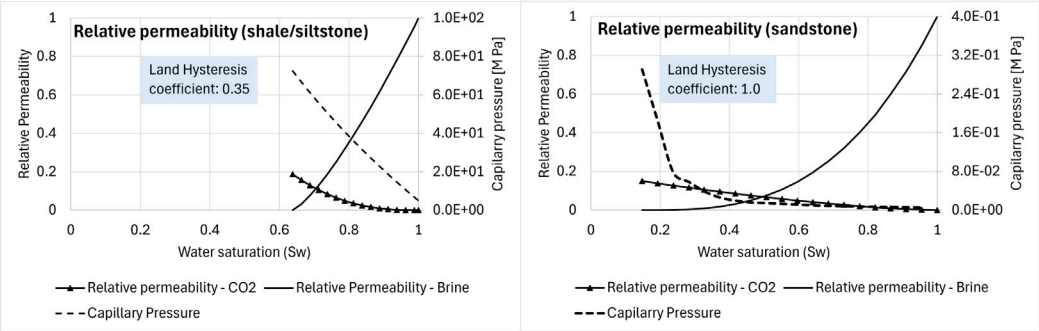


**Fig. 12.** Relative permeability curves, capillary pressure curve, and Land coefficient for shale and siltstone (left) and for sandstone (right).

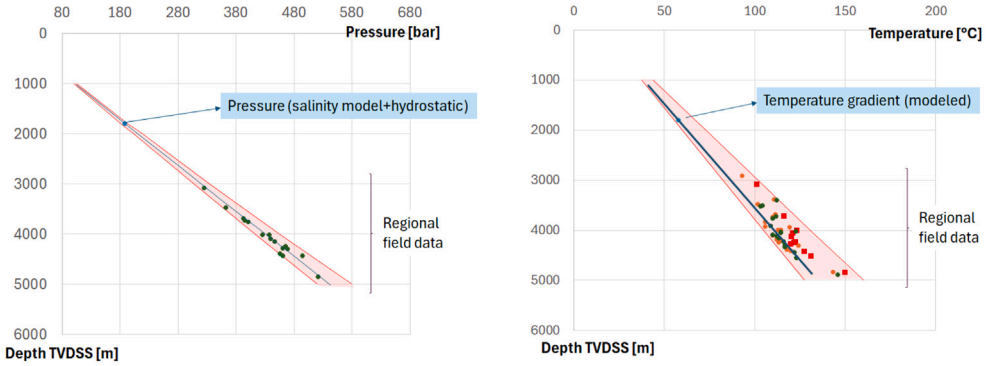


**Fig. 13.** Comparison of the pressure (left) and temperature (right) gradients observed in the aquifer and in the model.

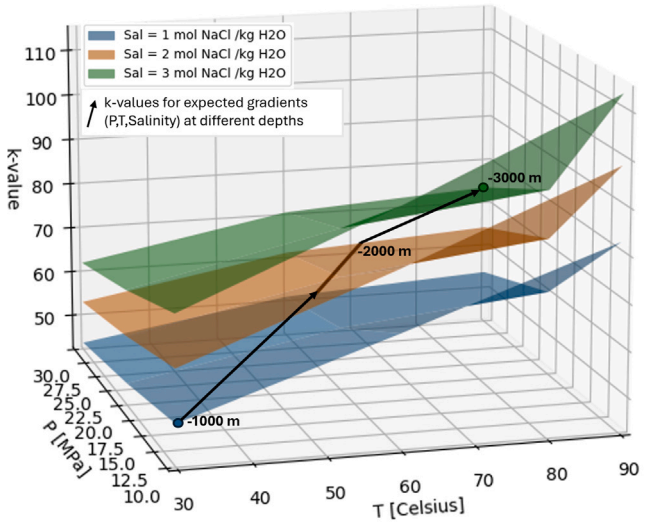


**Fig. 14.** k-values as a function of pressure, temperature and salinity (produced from the original solubility tables from Duan and Sun (2003)). Given the gradients, it is possible to estimate the trend of increased k-value (i.e., reduction of solubility) as depth increases.

The salinity and temperature gradients also cause a vertical gradient in $CO_2$-brine solubility. In the aquifer the solubility decreases with depth (Fig. 14), which is consistent with the results of other studies (Zhang et al., 2017; Addassi et al., 2022).

Finally, the hub scale (S4 to S3) consists of 8 clusters with 12 wells each. A hub with this well count is expected to have a capacity between 0.8 and 10 Gt using the simplified metrics proposed in ZEP (2011) of a storage capacity per offshore well between 8 and 104 Mt. This wide range was verified against different projects and studies (ZEP, 2011). For the cluster scale (S3 to S2), a single group with 12 wells was defined, which provides a capacity between 0.1 and 1.25 Gt using the same metric.

For each of these wells, the $CO_2$ injection is controlled by an injection pressure of 75 bar above the hydrostatic pressure at the level of the subsea wellheads located on the sea bed. This pressure was defined according to two criteria: first, $CO_2$ remains in supercritical conditions throughout the injection system assuming a minimum water depth of 200 m, and second, $CO_2$ can be provided by onshore compressors and pumps, located between 80 and 150 km from the injection groups.

To evaluate the reliability of $CO_2$ migration forecasts under different multiscale approaches, the key variable monitored is the percentage of $CO_2$ mass for each trapping mechanism, which ultimately defines storage security (Benson et al., 2005). If the mobile $CO_2$ content is smaller (because more of it is dissolved in brine or trapped by capillary forces), storage security increases. If a representation of an aquifer for a coarser grid predicts a higher solubility and/or more residual trapping than the fine grid version, it will be too optimistic, since it estimates a smaller mass of free $CO_2$ that can continue to migrate. The fine grid is assumed as reference for the transport solution, and thus for solubility and capillary trapping, too.

In summary, the results will be presented for four different test cases: Homogeneous reservoir (TC1); Representative Fluvio-Deltaic section (TC2); CCS with single well (TC3); CCS Cluster (TC4); CCS Hub (TC5). The Homogeneous and Fluvio-Deltaic cases compare all four strategies, as they were modeled and simulated in DARSim, which allows the evaluation of the ADM strategy. The CCS Cluster and the CCS Hub do not present the ADM results since they are not currently implemented in CMG-GEM. These test cases are listed in Table 4.

## 5. Results and discussion

The developed novel multiscale framework implies a cascading consistency check for the trapping mechanisms, from the well cluster

**Table 4**
Test cases defined to compare different strategies.

| Test case | Description | Simulator | Evaluated strategies |
|---|---|---|---|
| TC1 | Homogeneous reservoir, constant permeability and porosity | DARSim | upscaling, LGR, EV, ADM |
| TC2 | 2D section of a representative heterogeneous fluvio-deltaic saline aquifer | DARSim | upscaling, LGR, EV, ADM |
| TC3 | CCS with single well in a 16 km$^2$ area (simulation across S1 to S2 scales) | CMG-GEM | upscaling, LGR, EV |
| TC4 | CCS Cluster with 12 wells distributed over an area of 400 km$^2$, representative of Santos basin (simulation across S2 to S3 scales) | CMG-GEM | upscaling, LGR, EV |
| TC5 | CCS Hub with 96 wells distributed over an area of 40,000 km$^2$, representative of Santos basin (simulation across S3 to S4 scales) | CMG-GEM | upscaling, LGR, EV |

**Table 5**
Parameters transferred from larger scales to smaller scales, as boundary conditions. As boundaries get smaller, it is expected that the global productivity of the boundary gets smaller, too. The connected volume shows the localized limits for pressure dissipation. The volume of the S4 basin scale aquifer is estimated in 10 000 Gm$^3$.

| | $J_w$ [m$^3$/d/kPa] | $V_{out}$ [G m$^3$] |
|---|---|---|
| S4 (sealing boundaries) | – | – |
| S3 (transferred from S4) | 30 000 | 1000 |
| S2 (transferred from S3) | 20 000 | 1000 |
| S1 (transferred from S2) | 80 | 200 |

scale (S2), passing through the hub scale (S3) to the regional scale (S4). Simultaneously, in the other direction, from S4 to S2, the pressure consistency check requires the definition of the boundary flow conditions, in terms of the Fetkovich total productivity index $J_w$ and the connected boundary volume $V_{out}$ (see Table 5). The consistency check is a necessary element in the multiscale framework to ensure that the models are representative of the same storage conditions on all scales.

The effect of the proposed solutions for consistency on the trapping mechanisms (upscaling, LGR, EV, ADM) for each test case is presented in details in this section.

The homogeneous case TC1 highlights that overestimation occurs even in an ideal situation (see Fig. 15). In other words, it is possible to conclude that the numerical dispersion will be present in the upscaled simulations. When comparing two different scales, it is assumed that they are consistent if the predictions of the contribution of trapping mechanisms are in a range of ±1% (which is the precision required for fluid measurement by regulation in Brazil). Although the solubility mechanism was overstated by the coarsening of the grid, the residual trapping changes remain within the acceptance range. Considering that the representation of heterogeneities is relevant to residual trapping, it is expected that homogeneous cases would not suffer much from the upscaled one. The LGR, EV, and ADM proved effective methods in solving the overstated solubility mechanism in this case.

In a more complex setting, such as TC2, it is possible to observe deviations of the contributions of residual trapping (See Fig. 16). The detail lost during the upscaling process in a heterogeneous reservoir resulted in an overestimation of residual trapping as well, adding to the existing overestimation of solubility trapping. LGR, EV and ADM yielded results that were closer to the fine scale solution. As for TC1, LGR was applied with a refining ratio of 3.

For a single well injection as presented in TC3, almost all strategies are within the defined limits for the representation of the trapping mechanisms (see Fig. 17). The only exception is the conventional upscaling, that overstates the solubility mechanism. However, the difference was relatively small compared to other test cases, indicating that the S1 to S2 cell sizes may reproduce with more stability the trapping mechanisms.

For TC4, as presented in Fig. 18, the solubility is overestimated by conventional upscaling, while residual trapping remains acceptable. This indicates that the heterogeneity captured in the fine-scale model is still represented on the coarse scale. LGR fails to provide a good representation of both residual and solubility trapping, since the match of one of them leads to a mismatch in the other contribution. The matching of residual trapping, for instance, produced an underestimation of the solubility when comparing the LGR to the fine-scale solution. This illustrates the difficulties of applying LGR to accurately model both solubility and residual trapping since a higher degree of refinement does not necessarily produce a better representation of both mechanisms simultaneously. The overcompensation of solubility appeared with a refinement ratio of 2, smaller than the upscaling ratio of 3, and even higher error was found when increased refinements were tested. EV was able to reduce the error so that it remained within the target range. The possibility for the EV strategy to define an independent parameter for each trapping mechanism ($\alpha$ for solubility and $\beta$ for capillary trapping) was important to obtain this result.

Lastly, as demonstrated in Fig. 19, in TC5, both mechanisms are overestimated when using traditional upscaling methods. More precisely, LGR was unable to model with sufficient accuracy, leading to deviations, even using refinement ratios of 4. EV is still effective, but the limits of this approach start emerging, as the percentage of mass in the solubility trapping at the start of the post-injection period is below fine-grid solution and at the end of the period it is above.

Table 6 presents the summary of the differences for the estimated percentages of trapped $CO_2$ at the end of the observation period, comparing the larger to the smaller scales.

A summary of the numerical performance of the different strategies is presented in Table 7. Performance analysis is not in the objectives of this work, but it is nevertheless relevant since it defines some limits on the application of the models. The results are in line with the expected scenarios, with upscaling strategies reducing computational time. LGR improves performance from the fine models but is sometimes significantly higher than the upscaled models. The performance of EV is equivalent to the upscaling strategy, except for some eventual convergence issues that arise and can potentially increase the total time. Finally, ADM has an intermediate performance, between fine model and upscaling strategies performance. In general, it is possible to say that the results are in line with expectations.

Beyond the performance improvements, these results show the importance of checking the consistency of the representation of the trapping mechanisms across scales to validate the multiscale procedure. The resolution of the fluid distribution is clearly higher in smaller scales, as presented in Figs. 20 and 21. In addition, as shown in Fig. 22 for a 2D cross-section, the dissolved $CO_2$ plume and its saturation front spread over an extended region in the coarse grids, which can lead to wrong estimation of the trapped phase.

A specific discussion about the results for each strategy will be provided in the next subsections.

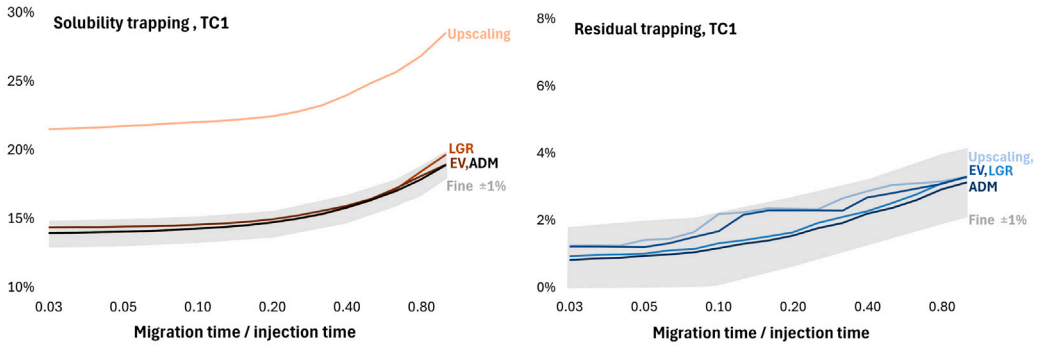


**Fig. 15.** The amount of solubility (left) and residual (right) trapping of $CO_2$ for TC1 for different upscaling methods. An acceptable upscaling solution should yield results that are within 1% of the fine-scale solution. The solubility is overestimated for the upscaling approach, while residual trapping is within target range.

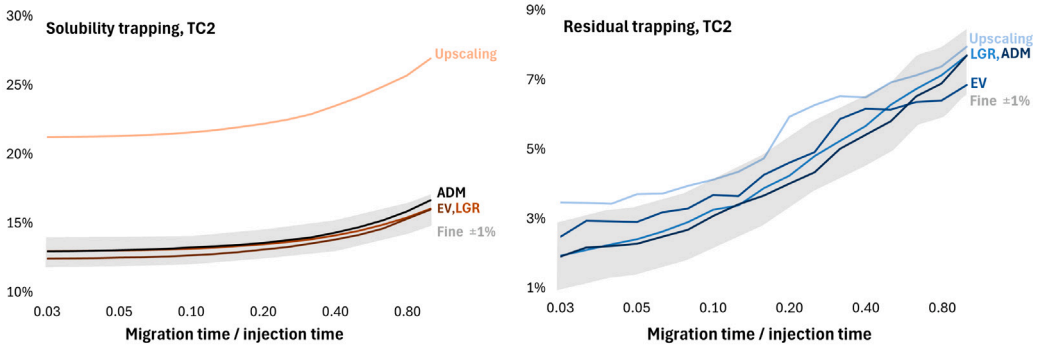


**Fig. 16.** The amount of solubility (left) and residual (right) trapping of $CO_2$ for TC2 for different upscaling methods. An acceptable upscaling solution should yield results that are within 1% of the fine-scale solution. Traditional upscaling strategy overestimates solubility and residual trapping.

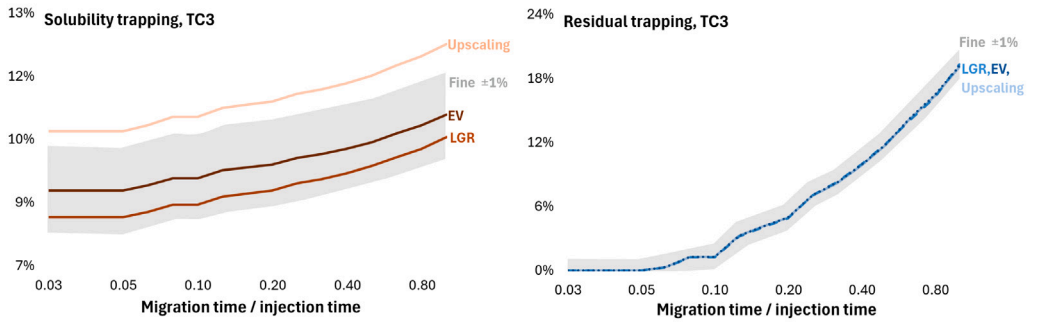


**Fig. 17.** The amount of solubility (left) and residual (right) trapping of $CO_2$ for TC3 for different upscaling methods. An acceptable upscaling solution should yield results that are within 1% of the fine-scale solution. Traditional upscaling strategy overestimates solubility, while residual trapping is within target range, with little variation across strategies.

*Upscaling*

There is a general bias in the representation of the trapping mechanism when using upscaled models: coarser grids lead to an overestimation of the solubility and residual $CO_2$ trapping mechanisms, reducing the total amount of free $CO_2$ migrating in the reservoir. This overestimation is problematic because it can lead to overly optimistic estimates of the trapping security in simplified models, which is the opposite of a robust design practice.

The overestimation observed in coarser grids is a numerical artifact that overstates the relevance of trapping mechanisms and has been observed by other authors in other scenarios (Pickup et al., 2010; Ukaegbu et al., 2009; Doughty and Pruess, 2003), and was observed to be present even in a homogeneous scenario.

In coarser grids, the contrast of small volume of injected $CO_2$ and large volume of in-situ brine in a single cell result in non-physical, fast and effective trapping mechanisms because low $CO_2$ volumes are in contact with much larger volumes of water (solubility trapping) and rock pore volumes (residual trapping), delaying the time in which the cells reach the saturation required to overcome the solubility limit. The overestimation of residual trapping seems higher for larger scales due to the facies upscaling.

*Local grid refinement*

LGR refines the coarse grid into smaller cells in areas where the petrophysical properties and/or state variables change quickly to reduce the solution errors. However, for $CO_2$ storage simulations, this

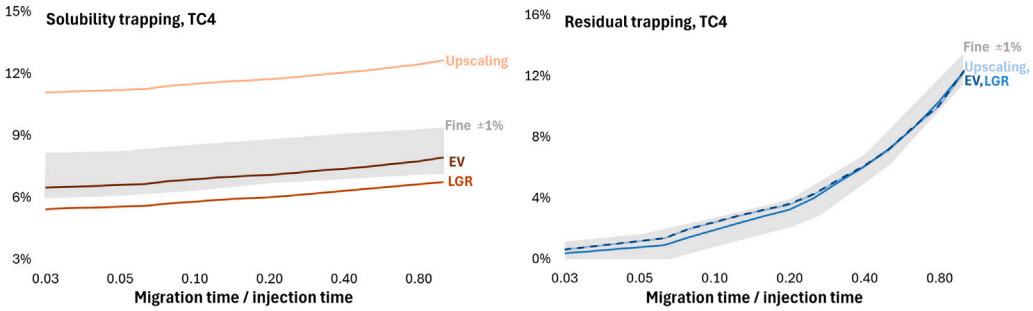


**Fig. 18.** The amount of solubility (left) and residual (right) trapping of $CO_2$ for TC4 for different upscaling methods. An acceptable upscaling solution should yield results that are within 1% of the fine-scale solution. Traditional upscaling strategy clearly overestimates solubility, while residual trapping is within target range.

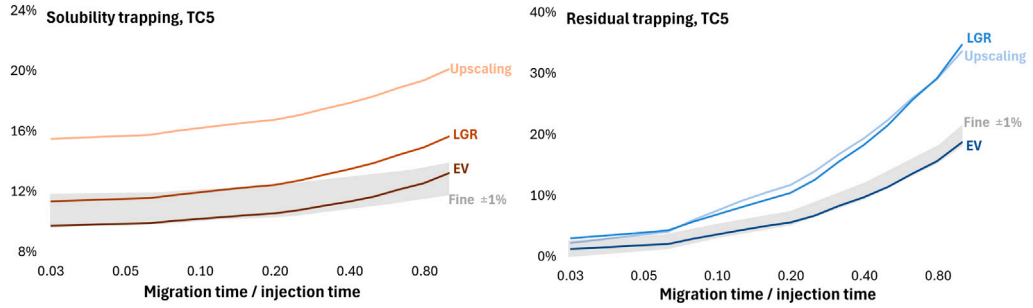


**Fig. 19.** The amount of solubility (left) and residual (right) trapping of $CO_2$ for TC5 for different upscaling methods. An acceptable upscaling solution should yield results that are within 1% of the fine-scale solution. Traditional upscaling strategy clearly overestimates both effects.

**Table 6**
Summary of the differences to the fine-scale model at the end of the injection and migration period. Acceptable values (within the range of ±1%) are in bold face.

| Test case/Strategy | Difference from fine, solubility trapping | Difference from fine, residual trapping | Upscaling strategy |
|---|---|---|---|
| TC1 upscaling | 9.6% | 0.2% | (3,3) upscaling ratio in x,y direction |
| **TC1 LGR** | **0.8%** | **0.2%** | Injection area refined at (3,3) ratio in x,y direction |
| **TC1 EV** | **0.1%** | **0.2%** | k-Value multiplier $\alpha = 1.7$; C(Land) multiplier $\beta = 1.05$ |
| **TC1 ADM** | **0.01%** | **0.02%** | 2 multiscale levels of (3,3) coarse-to-fine ratio in x,y direction (total ratio of (9,9)) |
| TC2 upscaling | 11.0% | 0.5% | (3,3) upscaling ratio in x,y direction |
| **TC2 LGR** | **0.1%** | **0.3%** | Injection area refined at (3,3) ratio in x,y direction |
| **TC2 EV** | **0.04%** | **−0.6%** | $\alpha = 2.0$; $\beta = 1.2$ |
| **TC2 ADM** | **0.7%** | **0.3%** | 2 multiscale levels of (3,3) coarse-to-fine ratio in x,y direction (total ratio of (9,9)) |
| TC3 upscaling | 1.6% | −0.5% | (3,3,3) upscaling ratio in x,y,z direction from S1 |
| TC3 LGR | **−0.6%** | **−0.2%** | Cluster area refined at (2,2,2) ratio in x,y direction |
| **TC3 EV** | **−0.1%** | **−0.4%** | $\alpha = 1.2$; $\beta = 1.0$ |
| TC4 upscaling | 4.4% | −0.5% | (3,3,2) upscaling ratio in x,y,z direction from S2 |
| TC4 LGR | −1.5% | −0.5% | Cluster area refined at (2,2,1) ratio in x,y direction |
| **TC4 EV** | **−0.3%** | **−0.4%** | $\alpha = 1.1$; $\beta = 1.0$ |
| TC5 upscaling | 7.4% | 13.6% | (4,4,3) upscaling ratio in x,y,z direction upscaling ratio from S3 |
| TC5 LGR | 2.9% | 14.7% | Hub area refined at (4,4,2) ratio in x,y direction |
| **TC5 EV** | **0.5%** | **−0.9%** | $\alpha = 2.2$; $\beta = 3.0$ |

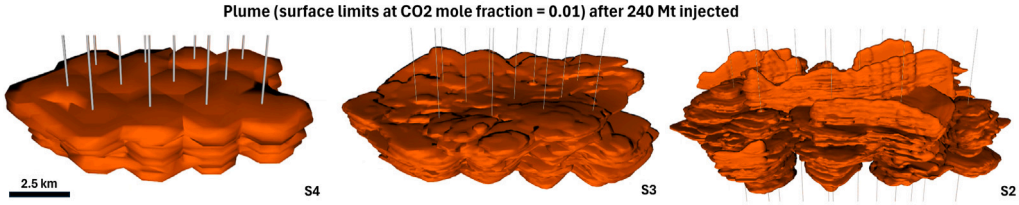


**Fig. 20.** Plume representation on three different scales providing increasing level of details for the same injection wells pattern. S4 (left) is a coarse model of S3 (center), which is a coarse model of S2 (right).

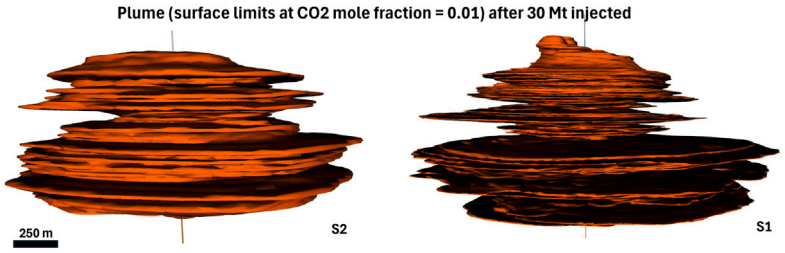


**Fig. 21.** Plume representation on two different scales providing increasing level of details for a single well. S2 (left) is a coarse model of S1 (right).

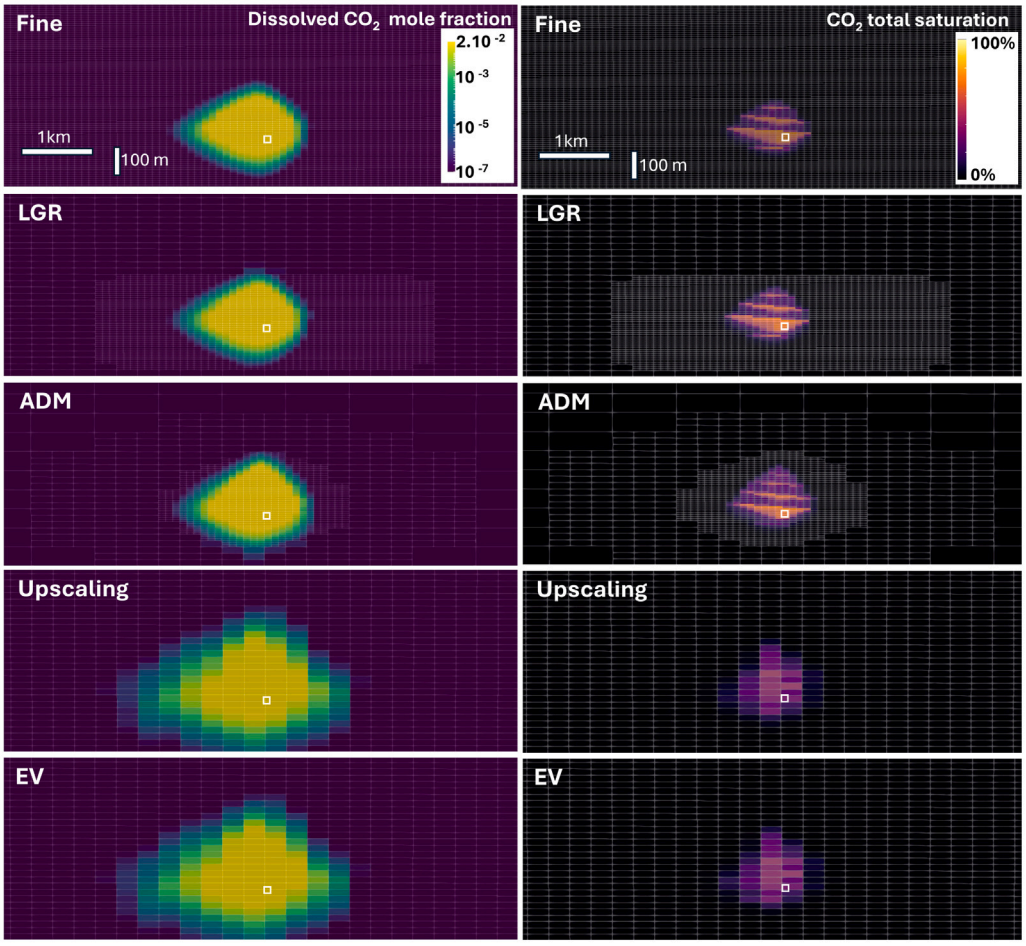


**Fig. 22.** 2D cross section of the plume on the injection region (highlighted by the white-lined box) of a selected well, comparing different strategies (plumes for dissolved $CO_2$ in brine and total $CO_2$ saturation), at the end of the migration period. The loss of resolution for upscaling and EV strategies leads to smeared out fronts for dissolved $CO_2$. Note that the dissolved $CO_2$ values are plotted in log scale, to enhance the visibility.

**Table 7**
Elapsed time in hours for the test cases and strategies. EV generally delivers performance near upscaled models, and LGR generally provides good performance. As for ADM, it is expected to have something between fine and upscaled model run time. 96.8% average parallel efficiency was achieved in multicore runs.

| Case | Runtime in hours | | | | | Description |
|---|---|---|---|---|---|---|
| | Fine | Upscaling | LGR | EV | ADM | |
| TC1 | 2.2 | 1.1 | 1.3 | 1.6 | 1.8 | DARSim, single core |
| TC2 | 2.9 | 1.3 | 1.8 | 1.3 | 2.1 | DARSim, single core |
| TC3 | 60 | 3.2 | 50 | 3.2 | – | CMG-GEM, 64 cores |
| TC4 | 423.4 | 58.1 | 112.5 | 58.3 | – | CMG-GEM, 64 cores |
| TC5 | 166.1 | 12.6 | 18.9 | 34.0 | – | CMG-GEM, 64 cores |

approach produces different results for each trapping mechanism, and the unbalanced results in complex settings made it difficult to consistently provide a good result. This translated into deviations from the fine model, delivering mixed results. Adding to the situation, higher levels of refinement produce a significant performance cost (a topic that is not within the scope of this paper), so it seems like a strategy that is applicable only in specific cases.

*Effective values*

For EV on $CO_2$ trapping mechanisms, two multipliers were defined, one for the solubility parameterization and one for residual trapping, providing the minimum degree of freedom necessary to match the fine-grid solution. The limitation of this solution is that there is no guarantee that the scaling constant remains the same if the original model conditions change (in terms of shale/permeability distribution or geometry, for example), so the best fit should be made for each pair of coarse-fine models. EV provides consistent results across all models, but parameterization is not directly obvious. The procedure applied for the definition of the EV multiplier was to apply the grid upscale ratio as a first (and pessimistic) guess and follow progressive reductions with a match procedure, although there are more sophisticated approaches to determine effective values for k-values (Salehi et al., 2019).

*Algebraic dynamic multilevel method (ADM)*

Finally, the last strategy, ADM, does not depend on the model characteristics and does not require a best-fit procedure, since it is adaptive and has a controlled error from the fine-grid solution. In general, it could avoid the performance issues observed in LGR, since only cells that exceed the variation threshold would need to be solved in fine grid resolution (in general, this amounts to 10%–30% of the cells). The ADM strategy requires a given hierarchical coarser grids imposed on the given fine grid over which multi-level basis functions are locally computed. These basis functions are indeed computed algebraically, making it convenient for integration with commercial simulators. Extensions to complex grids and parallel processing also requires more developments before it can be fully integrated into a commercial simulator.

ADM delivered good results, in line with the fine-grid trapping mechanism forecasts, even considering two multiscale levels (for a total of 9:1 coarse-to-fine ratio). This was a natural result because the ADM strategy populates the grid with fine properties for saturation and pressures, allowing hysteresis and solubility to be computed in fine-grid resolution despite resolving the pressure-transport equations in a coarse grid whenever possible.

*General discussion and limitations*

In summary, it is possible to observe a biased overestimation of the mechanisms as a result of upscale. LGR could not solve the problem for all the proposed scenarios and, while EV proved effective, it needed case-by-case parameterization and no general rule for this parameterization could be found. The ADM, on the other hand, does not require parameter tuning and, in essence, proposes the same strategy that is used to cope with heterogeneity and poropermeability representation: compute in fine resolution when needed, which is a robust approach to control the trapping mechanisms prediction error.

However, some assumptions of our approach limit the generalization of the results. To confirm the effectiveness of the methods for real field applications, more complex grid geometries specially corner-point grids need to be considered. In addition, high permeability contrasts including heterogeneous fractures and thermo-mechanical deformation and transport effects need to be also incorporated in the ADM (HosseiniMehr et al., 2020). These developments are the focus of our current studies.

Additionally, the longer term participation of trapping mechanisms is also relevant for carbon storage projects and therefore is a theme that requires further exploration. This work focused on the first 40 years of post-injection migration, which covers a relevant part of planned monitoring activities, but it is known that the full cycle of a carbon storage project easily covers hundreds of years. To fully access storage safety, this longer period must also be evaluated. A multi-scale in time has to be developed to complement our spatial multiscale framework (Delpopolo Carciopolo et al., 2020b,a). This is another topic of our future research.

## 6. Conclusions

Giant saline aquifers are very attractive candidates for $CO_2$ storage. Effective storage of $CO_2$ is these fields depends also on reliable assessments of the plume dynamics based on accurate numerical simulations. However, simulation of $CO_2$ plume dynamics in these giant systems is significantly challenging, due to the size of the system with high-resolution heterogeneous properties and nonlinear complex $CO_2$/Brine/Rock properties. To reduce the computational complexities, classically upscaled models on coarser resolution grids are employed. However, this introduces significant errors in the assessment of trapped and mobile $CO_2$ mass. This motivates the development of advanced simulation strategies that maintain computational efficiency and the expected accuracy.

In this work, first, we developed a multiscale framework that allows global solutions to be used as boundary conditions on smaller localized systems. These systems are hierarchically connected to each other, from the well-scale system S1 to the most global domain of S4. This strategy allowed for proper addressing of the global pressure, which affects physical terms such as solubility, across all of the system resolutions. As for the transport, i.e., local unknown, each system is expected to solve the multiphase flow system appropriately once the boundary conditions are defined from the lower resolution system.

As a second development of this study, for the well cluster domain, i.e. S2, three different multiscale simulation methods were utilized, which are: LGR, EV, and ADM. Through several systematic analyses, it was found that the EV is highly sensitive to the parameter calibration stage and can only be used once a reference system can be obtained. LGR, on the other hand, was found to be more generic with the limitation of the need for upscaling the transmissibility field. However, ADM was found to be the most generic method that systematically resulted in reliable and efficient solutions on a representative section of the field. The extension of ADM method for allowing its full-field deployment is a promising future development, which might confirm the findings in a more general context. Our findings were confirmed by applying different methods on the Santos basin storage case in Brazil. We have found an operational method (EV) that is compatible with all commercial software, and a promising method (ADM) that might improve the representation of plume and pressure behavior.

Based on these findings, we recommend the generalization of ADM for field-scale simulations, and careful verification of the integrity of trapping mechanisms representation when simplification methods are applied. Future studies will include sensitivity analyses and multiscale data integration within our multiscale framework.

## CRediT authorship contribution statement

**Mathias José Kreutz Erdtmann:** Writing – original draft, Visualization, Software, Methodology, Conceptualization. **Filipe Silva Lira:** Writing – review & editing, Visualization, Resources, Investigation, Data curation. **Sebastian Geiger:** Writing – review & editing, Methodology. **Hadi Hajibeygi:** Writing – review & editing, Supervision, Methodology, Conceptualization.

## Declaration of competing interest

The authors declare that they have no known competing financial interests or personal relationships that could have appeared to influence the work reported in this paper.

## Acknowledgments

The authors acknowledge Petróleo Brasileiro SA (Petrobras) for supporting this research and Computer Modelling Group (CMG) for providing the software packages needed to conduct the test cases. The simulations implemented in DARSim test cases are made available to the public in the open source Delft Advanced Reservoir Simulator (DARSim) (Delft Advanced Reservoir Simulator (DARSIM), 2024). Sebastian Geiger and Hadi Hajibeygi acknowledge Energi Simulation for supporting their chairs.

## Data availability

The simulations implemented in DARSim test cases are made available to the public in the open source Delft Advanced Reservoir Simulator (DARSim)

## References

Addassi, M., Omar, A., Hoteit, H., et al., 2022. Assessing the potential of solubility trapping in unconfined aquifers for subsurface carbon storage. Nat. Sci. Rep. 12, http://dx.doi.org/10.1038/s41598-022-24623-6.

AL homoud, R., Machado, M.V.B., Daigle, H., Sepehrnoori, K., Ates, H., 2024. Impact of wettability and relative permeability hysteresis in saline aquifers; implication of hydrogen underground storage. SPE West. Reg. Meet. http://dx.doi.org/10.2118/218942-MS, D021S011R004.

Alamara, H., Blondeau, C., Thibeau, S., Bogdanov, I., 2025. Vertical equilibrium simulation for industrial-scale CO2 storage in heterogeneous aquifers. Sci. Rep. 15, http://dx.doi.org/10.1038/s41598-025-00751-7.

Alipour K., M., Kasha, A., Sakhaee-Pour, A., Sadooni, F.N., Al-Kuwari, H.A.-S., 2022. Empirical relation for capillary pressure in shale. Petrophysics - SPWLA J. 63 (05), 591–603. http://dx.doi.org/10.30632/PJV63N5-2022a2.

Amarante, F.B.D., Kuchle, J., Scherer, C.M.D.S., Dashtgard, S.E., Haag, M.B., 2024. Geological screening of onshore saline aquifers for CO2 storage: Paraná and Espírito Santo basins, Brazil. Adv. Geosci. 65, 19–35. http://dx.doi.org/10.5194/adgeo-65-19-2024.

Anjos, S.M.C., Sombra, C.L., Spadini, A.R., 2024. Petroleum exploration and production in Brazil: From onshore to ultra-deepwaters. Pet. Explor. Dev. 51 (4), 912–924. http://dx.doi.org/10.1016/S1876-3804(24)60515-X.

Awid, A., Geiger, S., Mackay, E., 2018. The impact of near-wellbore refinement on modelling advanced and smart well completions in reservoir simulation. SPE Kingdom of Saudi Arabia Annual Technical Symposium and Exhibition, SPE Kingd. Saudi Arab. Annu. Tech. Symp. Exhib. SPE Kingdom of Saudi Arabia Annual Technical Symposium and Exhibition, SPE–192253–MS. http://dx.doi.org/10.2118/192253-MS.URL https://doi.org/10.2118/192253-MS,

Bacoccoli, G., Gamarra Morales, R., Morgado de Castro, P.J., 1979. Oil exploration in campos Basin, Brazil; model for exploration in Atlantic-type basins. In: AAPG Bulletin, vol. 63, American Association of Petroleum Geologists, p. 412, Abstract. URL http://pubs.geoscienceworld.org/aapg/aapgbull/article-pdf/63/3/412/4447967/aapg_1979_0063_0003_0412a.pdf.

Bandilla, K.W., Guo, B., Celia, M.A., 2019. A guideline for appropriate application of vertically-integrated modeling approaches for geologic carbon storage modeling. Int. J. Greenh. Gas Control. 91, 102808. http://dx.doi.org/10.1016/j.ijggc.2019.102808, URL https://www.sciencedirect.com/science/article/pii/S1750583619300684.

Barbosa Machado, M.V., Delshad, M., Sepehrnoori, K., 2024. A computationally efficient approach to model reactive transport during CO2 storage in naturally fractured saline aquifers. Geoenergy Sci. Eng. 236, 212768. http://dx.doi.org/10.1016/j.geoen.2024.212768.

Barker, J.W., Dupouy, P., 1999. An analysis of dynamic pseudo-relative permeability methods for oil-water flows. Pet. Geosci. 5 (4), 385–394. http://dx.doi.org/10.1144/petgeo.5.4.385.

Benson, S., Abanades, J.C., Akai, M., Caldeira, K., Cook, P., Davidson, O., Doctor, R., Dooley, J., Freund, P., Gale, J., Heidug, W., Herzog, H., Keith, D., Mazzotti, M., Metz, B., Osman-Elasha, B., Palmer, A., Pipatti, R., Smekens, K., Soltanieh, M., Thambimuthu, K., van der Zwaan, B., 2005. IPCC Spec. Repot Carbon Capture Storage 195–276, URL https://cir.nii.ac.jp/crid/1573387450727411840.

Bentley, M., Stephens, E., 2026. Storage v. production: challenges for reservoir modelling and simulation practitioners. Energy Geosci. Conf. Ser. 1 (1), egc1–2024–67. http://dx.doi.org/10.1144/egc1-2024-67.

Buntic, I., Schneider, M., Flemisch, B., Helmig, R., 2025. A fully-implicit solving approach to an adaptive multi-scale model - coupling a vertical-equilibrium and full-dimensional model for compressible, multi-phase flow in porous media. Comput. Geosci. 29 (2), 11. http://dx.doi.org/10.1007/s10596-025-10351-z.

Burnside, N., Naylor, M., 2014. Review and implications of relative permeability of CO2/brine systems and residual trapping of CO2. Int. J. Greenh. Gas Control. 23, 1–11. http://dx.doi.org/10.1016/j.ijggc.2014.01.013.

Celia, M.A., Bachu, S., Nordbotten, J.M., Bandilla, K.W., 2015. Status of CO2 storage in deep saline aquifers with emphasis on modeling approaches and practical simulations. Water Resour. Res. 51 (9), 6846–6892. http://dx.doi.org/10.1002/2015WR017609, URL https://agupubs.onlinelibrary.wiley.com/doi/abs/10.1002/2015WR017609.

Christie, M.A., Blunt, M.J., 2001. Tenth SPE comparative solution project: A comparison of upscaling techniques. SPE Reservoir Simulation Conference, SPE Reserv. Simul. Symp. SPE Reservoir Simulation Conference, SPE–66599–MS.http://dx.doi.org/10.2118/66599-MS,

Computer Modelling Group Ltd., 2024. GEM compositional & unconventional simulator. Version 2024.10, Software for compositional and unconventional reservoir simulation. URL https://www.cmgl.ca/software/gem.

Court, B., Bandilla, K.W., Celia, M.A., Janzen, A., Dobossy, M., Nordbotten, J.M., 2012. Applicability of vertical-equilibrium and sharp-interface assumptions in CO2 sequestration modeling. Int. J. Greenh. Gas Control. 10, 134–147. http://dx.doi.org/10.1016/j.ijggc.2012.04.015, URL https://www.sciencedirect.com/science/article/pii/S1750583612001041.

Cusini, M., van Kruijsdijk, C., Hajibeygi, H., 2016. Algebraic dynamic multilevel (ADM) method for fully implicit simulations of multiphase flow in porous media. J. Comput. Phys. 314, 60–79. http://dx.doi.org/10.1016/j.jcp.2016.03.007.

Dahle, H.K., Espedal, M.S., Sæ vareid, O., 1992. Characteristic, local grid refinement techniques for reservoir flow problems. Internat. J. Numer. Methods Engrg. 34 (3), 1051–1069. http://dx.doi.org/10.1002/nme.1620340324, URL https://onlinelibrary.wiley.com/doi/abs/10.1002/nme.1620340324.

de Oliveira, S.B., Weber, N., Yeates, C., Tassinari, C.C.G., 2023. Geological screening for onshore CO2 storage in the Rio Bonito formation, Paraná Basin, Brazil. J. Maps 19 (1), 2171817. http://dx.doi.org/10.1080/17445647.2023.2171817.

Delft Advanced Reservoir Simulator (DARSIM), 2024. DARSIM: Delft Advanced Reservoir Simulator. URL https://gitlab.com/darsim.

Delpopolo Carciopolo, L., Cusini, M., Formaggia, L., Hajibeygi, H., 2020a. Adaptive multilevel space-time-stepping scheme for transport in heterogeneous porous media (ADM-LTS). J. Comput. Phys.: X 6, 100052. http://dx.doi.org/10.1016/j.jcpx.2020.100052, URL https://www.sciencedirect.com/science/article/pii/S2590055220300044.

Delpopolo Carciopolo, L., Formaggia, L., Scotti, A., Hajibeygi, H., 2020b. Conservative multirate multiscale simulation of multiphase flow in heterogeneous porous media. J. Comput. Phys. 404, 109134. http://dx.doi.org/10.1016/j.jcp.2019.109134, URL https://www.sciencedirect.com/science/article/pii/S0021999119308393.

Doster, F., Nordbotten, J., Celia, M., 2013. Impact of capillary hysteresis and trapping on vertically integrated models for CO2 storage. Adv. Water Resour. 62, 465–474. http://dx.doi.org/10.1016/j.advwatres.2013.09.005, Computational Methods in Geologic CO2 Sequestration. URL https://www.sciencedirect.com/science/article/pii/S0309170813001577.

Doughty, C., Pruess, K., 2003. Modeling supercritical CO2 injection in heterogeneous porous media. In: Proceedings of the TOUGH Symposium 2003.

Duan, Z., Sun, R., 2003. An improved model calculating CO2 solubility in pure water and aqueous NaCl solutions from 273 to 533 k and from 0 to 2000 bar. Chem. Geol. 193 (3), 257–271. http://dx.doi.org/10.1016/S0009-2541(02)00263-2.

Dunk, R., Aiken, T., Widdicombe, S., Hovland, M., Brewer, P., Vivian, C., 2008. Assessment of Sub Sea Ecosystem Impacts. Technical Report 2008/8, IEA Greenhouse Gas R&D Programme, Cheltenham, UK, URL https://www.ieaghg.org.

Durlofsky, L.J., 1991. Numerical calculation of equivalent grid block permeability tensors for heterogeneous porous media. Water Resour. Res. 27 (5), 699–708. http://dx.doi.org/10.1029/91WR00107.

Durlofsky, L.J., 2005. Upscaling and gridding of fine scale geological models for flow simulation. In: 8th International Forum on Reservoir Simulation Iles Borromees, Stresa, Italy. pp. 1–59.

Durlofsky, L.J., Chen, Y., 2012. Uncertainty quantification for subsurface flow problems using coarse-scale models. In: Numerical Analysis of Multiscale Problems. Springer Berlin Heidelberg, Berlin, Heidelberg, pp. 163–202. http://dx.doi.org/10.1007/978-3-642-22061-6_6.

Farmer, C.L., 2002. Upscaling: a review. Internat. J. Numer. Methods Fluids 40 (1–2), 63–78. http://dx.doi.org/10.1002/fld.267.

Fetkovich, M., 1971. A simplified approach to water influx calculations-finite aquifer systems. J. Pet. Technol. 23 (07), 814–828. http://dx.doi.org/10.2118/2603-PA.

Flemisch, B., Nordbotten, J.M., Fernø, M., Juanes, R., Both, J.W., Class, H., Delshad, M., Doster, F., Ennis-King, J., Franc, J., Geiger, S., Gläser, D., Green, C., Gunning, J., Hajibeygi, H., Jackson, S.J., Jammoul, M., Karra, S., Li, J., Matthäi, S.K., Miller, T., Shao, Q., Spurin, C., Stauffer, P., Tchelepi, H., Tian, X., Viswanathan, H., Voskov, D., Wang, Y., Wapperom, M., Wheeler, M.F., Wilkins, A., Youssef, A.A., Zhang, Z., 2024. The FluidFlower validation benchmark study for the storage of co$$_2$$. Transp. Porous Media 151 (5), 865–912. http://dx.doi.org/10.1007/s11242-023-01977-7.

Guo, B., Bandilla, K.W., Doster, F., Keilegavlen, E., Celia, M.A., 2014. A vertically integrated model with vertical dynamics for CO2 storage. Water Resour. Res. 50 (8), 6269–6284. http://dx.doi.org/10.1002/2013WR015215.

Hadjisotiriou, G., Sass, J., Wapperom, M., Novikov, A., Voskov, D.V., 2025. SPE11: Convergence study and extension to realistic physics. SPE Reserv. Simul. Conf. http://dx.doi.org/10.2118/223922-MS.

Hajibeygi, H., Bonfigli, G., Hesse, M.A., Jenny, P., 2008. Iterative multiscale finite-volume method. J. Comput. Phys. 227 (19), 8604–8621. http://dx.doi.org/10.1016/j.jcp.2008.06.013.

Hajibeygi, H., Karvounis, D., Jenny, P., 2011. A loosely coupled hierarchical fracture model for the iterative multiscale finite volume method. SPE Reserv. Simul. Conf. http://dx.doi.org/10.2118/141991-MS, SPE-141991-MS.

Hajibeygi, H., Olivares, M.B., HosseiniMehr, M., Pop, S., Wheeler, M., 2020. A benchmark study of the multiscale and homogenization methods for fully implicit multiphase flow simulations. Adv. Water Resour. 143, 103674. http://dx.doi.org/10.1016/j.advwatres.2020.103674.

HosseiniMehr, M., Vuik, C., Hajibeygi, H., 2020. Adaptive dynamic multilevel simulation of fractured geothermal reservoirs. J. Comput. Phys.: X 7, 100061. http://dx.doi.org/10.1016/j.jcpx.2020.100061, URL https://www.sciencedirect.com/science/article/pii/S2590055220300135.

Iglauer, S., 2011. Dissolution trapping of carbon dioxide in reservoir formation brine – a carbon storage mechanism. In: Nakajima, H. (Ed.), Mass Transfer. IntechOpen, Rijeka, http://dx.doi.org/10.5772/20206.

Instituto do Petróleo e dos Recursos Naturais (I.P.R. - PUCRS), 2025. Plataforma GIS CCUS brasil. URL https://www.pucrs.br/ipr/plataforma-gis-ccus-brasil/.

Juanes, R., Spiteri, E.J., Orr Jr., F.M., Blunt, M.J., 2006. Impact of relative permeability hysteresis on geological CO2 storage. Water Resour. Res. 42 (12), http://dx.doi.org/10.1029/2005WR004806, URL https://agupubs.onlinelibrary.wiley.com/doi/abs/10.1029/2005WR004806.

Kachuma, D., Hasanzade, R., Tomin, P., Thomadakis, M.E., Franc, J., Magri, V.A.P., Byer, T.J., Cusini, M., Settgast, R.R., Gross, H., Castelletto, N., 2026. High-resolution simulations of geological CO2 injection: Application to the SPE11 benchmark. SPE J. 31 (01), 680–696. http://dx.doi.org/10.2118/231182-PA.

King, M.J., Mansfield, M., 1999. Flow simulation of geologic models. SPE Reserv. Eval. Eng. 2 (04), 351–367. http://dx.doi.org/10.2118/57469-PA.

Krevor, S., Blunt, M.J., Benson, S.M., Pentland, C.H., Reynolds, C., Al-Menhali, A., Niu, B., 2015. Capillary trapping for geologic carbon dioxide storage – from pore scale physics to field scale implications. Int. J. Greenh. Gas Control. 40, 221–237. http://dx.doi.org/10.1016/j.ijggc.2015.04.006, Special Issue commemorating the 10th year anniversary of the publication of the Intergovernmental Panel on Climate Change Special Report on CO2 Capture and Storage.

Land, C.S., 1968. Calculation of imbibition relative permeability for two- and three-phase flow from rock properties. Soc. Pet. Eng. J. 8 (02), 149–156. http://dx.doi.org/10.2118/1942-PA.

Li, Y.-K., Nghiem, L.X., 1986. Phase equilibria of oil, gas and water/brine mixtures from a cubic equation of state and henry's law. Can. J. Chem. Eng. 64 (3), 486–496. http://dx.doi.org/10.1002/cjce.5450640319.

Lira, F.S., Erdtmann, M.J.K., Menezes, L., Bortolini, S., Guirro, A., Waisman, G., Bulhoes, F., Freitas, G., Vieira, G., Lima, N., Gantois, G., da Costa, F., Zerfass, H., Cassino, L., Walter, P., Martinius, A., Geiger, S., 2025. CO2 storage complex in santos basin, Brazil: Storage potential and impacts of heterogeneity in pressure front. World CCUS Conf. 2025.

Lopez-Saavedra, S., Bajestani, M.S., Pantov, D., Chalaturnyk, R., Zambrano-Narvaez, G., 2025. Hypergravity experiments on meter-scale porous media flow for geological carbon sequestration. Sci. Rep. 15 (1), 45712. http://dx.doi.org/10.1038/s41598-025-28226-9, URL https://doi.org/10.1038/s41598-025-28226-9.

Lyu, X., Voskov, D., 2023. Advanced modeling of enhanced CO2 dissolution trapping in saline aquifers. Int. J. Greenh. Gas Control. 127, 103907. http://dx.doi.org/10.1016/j.ijggc.2023.103907, URL https://www.sciencedirect.com/science/article/pii/S1750583623000774.

Michaud, M.C., Bisshopp, F., 1981. Accurate waterflood simulation using biased difference and selective grid refinement. Soc. Pet. Eng. AIME, Pap.; (United States) SPE-9799, URL https://www.osti.gov/biblio/6164441.

Mim, R.T., Negash, B.M., Jufar, S.R., Ali, F., 2023. Minireview on CO2 storage in deep saline aquifers: Methods, opportunities, challenges, and perspectives. Energy Fuels 37 (23), 18467–18484. http://dx.doi.org/10.1021/acs.energyfuels.3c03185.

Miotliński, K., Peeters, L.J.M., 2021. Quantification of carbon cycling in a large aquifer using reactive transport modelling. Front. Water 3, 714075. http://dx.doi.org/10.3389/frwa.2021.714075.

Misaghi Bonabi, A., van Rooijen, W., Al Kobaisi, M., Vuik, C., Hajibeygi, H., 2025. Comparative analysis of carbon dioxide and hydrogen plume migration in aquifers inspired by the FluidFlower benchmark study. Int. J. Hydrog. Energy 135, 56–68. http://dx.doi.org/10.1016/j.ijhydene.2025.04.401, URL https://www.sciencedirect.com/science/article/pii/S0360319925020944.

Ni, H., Li, B., Darraj, N., Ren, B., Harris, C., Krishnamurthy, P.G., Bukar, I., Berg, S., Snippe, J., Ringrose, P., Meckel, T., Krevor, S., Benson, S., 2025. The impact of capillary heterogeneity on CO2 flow and trapping across scales. Earth-Sci. Rev. 270, 105257. http://dx.doi.org/10.1016/j.earscirev.2025.105257.

Noetinger, B., Zargar, G., 2004. Multiscale description and upscaling of fluid flow in subsurface reservoirs. Oil Gas Sci. Technol. – Rev. D'IFP Energies Nouv. 59 (2), 119–139. http://dx.doi.org/10.2516/ogst:2004010.

Nordbotten, J.M., Ferno, M.A., Flemisch, B., Kovscek, A.R., Lie, K.-A., 2024. The 11th society of petroleum engineers comparative solution project: Problem definition. SPE J. 29 (05), 2507–2524. http://dx.doi.org/10.2118/218015-PA.

Nordbotten, J.M., Fernø, M.A., Flemisch, B., Kovscek, A.R., Lie, K.-A., Both, J.W., Møyner, O., Sandve, T.H., Ahusborde, E., Bauer, S., Chen, Z., Class, H., Di, C., Ding, D., Element, D., Flauraud, E., Franc, J., Gasanzade, F., Ghomian, Y., Giddins, M.A., Green, C., Fernandes, B.R., Hadjisotiriou, G., Hammond, G., Huang, H., Kachuma, D., Kern, M., Koch, T., Krishnamurthy, P., Lye, K.O., Landa-Marbán, D., Nole, M., Orsini, P., Ruby, N., Salinas, P., Sayyafzadeh, M., Torben, J., Turner, A., Voskov, D.V., Wendel, K., Youssef, A.A., 2025. Benchmarking CO2 storage simulations: Results from the 11th society of petroleum engineers comparative solution project. Int. J. Greenh. Gas Control. 148, 104519. http://dx.doi.org/10.1016/j.ijggc.2025.104519.

Nordbotten, J., Flemisch, B., Gasda, S., Nilsen, H., Fan, Y., Pickup, G., Wiese, B., Celia, M., Dahle, H., Eigestad, G., Pruess, K., 2012. Uncertainties in practical simulation of CO2 storage. Int. J. Greenh. Gas Control. 9, 234–242. http://dx.doi.org/10.1016/j.ijggc.2012.03.007.

Pau, G.S., Bell, J.B., Pruess, K., Almgren, A.S., Lijewski, M.J., Zhang, K., 2010. High-resolution simulation and characterization of density-driven flow in CO2 storage in saline aquifers. Adv. Water Resour. 33 (4), 443–455. http://dx.doi.org/10.1016/j.advwatres.2010.01.009, URL https://www.sciencedirect.com/science/article/pii/S0309170810000217.

Peaceman, D.W., 1983. Interpretation of well-block pressures in numerical reservoir simulation with nonsquare grid blocks and anisotropic permeability. Soc. Pet. Eng. J. 23 (03), 531–543. http://dx.doi.org/10.2118/10528-PA.

Pickup, G., Kiatsakulphan, M., Mills, J., 2010. Analysis of grid resolution for simulations of CO2 storage in deep saline aquifers. Proc. the 12th Eur. Conf. Math. Oil Recover. (ECMOR XII).

Pickup, G.E., Ringrose, P.S., Corbett, P.W.M., Jensen, J.L., Sorbie, K.S., 1994. Geology, geometry, and effective flow. SPE Annu. Tech. Conf. Exhib. SPE–28374–MS. http://dx.doi.org/10.2118/28374-MS.

Pour, K.M., Voskov, D., Bruhn, D., 2023. Nonlinear solver based on trust region approximation for CO2 utilization and storage in subsurface reservoir. Geoenergy Sci. Eng. 225, 211698. http://dx.doi.org/10.1016/j.geoen.2023.211698, URL https://www.sciencedirect.com/science/article/pii/S2949891023002853.

Rabinovich, A., Itthisawatpan, K., Durlofsky, L.J., 2015. Upscaling of CO2 injection into brine with capillary heterogeneity effects. J. Pet. Sci. Eng. 134, 60–75. http://dx.doi.org/10.1016/j.petrol.2015.07.021.

Ringrose, P., Bentley, M., 2021. Reservoir Model Design: A Practitioner's Guide, second ed. Springer, http://dx.doi.org/10.1007/978-3-030-70163-5.

Ringrose, P.S., Furre, A.-K., Gilfillan, S.M., Krevor, S., Landrø, M., Leslie, R., Meckel, T., Nazarian, B., Zahid, A., 2021. Storage of carbon dioxide in saline aquifers: Physicochemical processes, key constraints, and scale-up potential. "Annual Rev. Chem. Biomol. Engineering" 12 (Volume 12, 2021), 471–494. http://dx.doi.org/10.1146/annurev-chembioeng-093020-091447, URL https://www.annualreviews.org/content/journals/10.1146/annurev-chembioeng-093020-091447.

Rockett, G.C., Machado, C.X., Ketzer, J.M.M., Centeno, C.I., 2010. The CARBMAP project: Matching CO2 sources and geological sinks in Brazil using geographic information system. Energy Procedia.

Ruprecht, C., Pini, R., Falta, R., Benson, S., Murdoch, L., 2014. Hysteretic trapping and relative permeability of CO2 in sandstone at reservoir conditions. Int. J. Greenh. Gas Control. 27, 15–27. http://dx.doi.org/10.1016/j.ijggc.2014.05.003.

Salehi, A., Voskov, D.V., Tchelepi, H.A., 2019. K-values-based upscaling of compositional simulation. SPE J. 24 (02), 579–595. http://dx.doi.org/10.2118/182725-PA.

Shook, G.M., Mitchell, K.M., 2009. A robust measure of heterogeneity for ranking earth models: The F-PHI curve and dynamic lorenz coefficient. SPE Annu. Tech. Conf. Exhib. SPE–124625–MS. http://dx.doi.org/10.2118/124625-MS.

Sun, X., Wang, Z., Li, H., He, H., Sun, B., 2021. A simple model for the prediction of mutual solubility in CO2-brine system at geological conditions. Desalination 504, 114972. http://dx.doi.org/10.1016/j.desal.2021.114972.

Syrakos, A., Efthimiou, G., Bartzis, J.G., Goulas, A., 2012. Numerical experiments on the efficiency of local grid refinement based on truncation error estimates. J. Comput. Phys. 231 (20), 6725–6753. http://dx.doi.org/10.1016/j.jcp.2012.06.023.

Tveit, S., Gasda, S.E., Landa-Marbán, D., Sandve, T.H., 2025. A hierarchical approach for modeling regional pressure interference in multi-site CO2 operations. Geoenergy Sci. Eng. 248, 213733. http://dx.doi.org/10.1016/j.geoen.2025.213733, URL https://www.sciencedirect.com/science/article/pii/S2949891025000910.

Ukaegbu, C., Gundogan, O., Mackay, E., Pickup, G., Todd, A., Gozalpour, F., Burnard, K., 2009. Simulation of CO2 storage in a heterogeneous aquifer. Proc. Inst. Mech. Eng. Part A: J. Power Energy 223 (3), 249–267. http://dx.doi.org/10.1243/09576509JPE627.

Wang, Y., Vuik, C., Hajibeygi, H., 2022. Analysis of hydrodynamic trapping interactions during full-cycle injection and migration of CO2 in deep saline aquifers. Adv. Water Resour. 159, 104073. http://dx.doi.org/10.1016/j.advwatres.2021.104073.

Wang, Y., Zhang, Z., Vuik, C., Hajibeygi, H., 2024. Simulation of CO2 storage using a parameterization method for essential trapping physics: FluidFlower benchmark study. Transp. Porous Media 151 (5), 1053–1070. http://dx.doi.org/10.1007/s11242-023-01987-5, URL https://doi.org/10.1007/s11242-023-01987-5.

Wenck, N., Muggeridge, A., Jackson, S., An, S., Krevor, S., 2024. The impact of capillary heterogeneity on CO2 plume migration at the endurance CO2 storage site in the UK. Geoenergy http://dx.doi.org/10.1144/geoenergy2024-029.

ZEP, 2011. The Costs of $CO_2$ Storage: Post-Demonstration CCS in the EU. Technical Report, European Technology Platform for Zero Emission Fossil Fuel Power Plants, Brussels, Belgium.

Zhang, Q., Geiger, S., Storms, J.E., Voskov, D.V., Jackson, M.D., Hampson, G.J., Jacquemyn, C., Martinius, A.W., 2025. Capillary pinning in sedimentary rocks for CO2 storage: Mechanisms, terminology and state-of-the-art. Int. J. Greenh. Gas Control. 144, 104385. http://dx.doi.org/10.1016/j.ijggc.2025.104385.

Zhang, Y., Lashgari, H.R., Sepehrnoori, K., Di, Y., 2017. Effect of capillary pressure and salinity on CO2 solubility in brine aquifers. Int. J. Greenh. Gas Control. 57, 26–33. http://dx.doi.org/10.1016/j.ijggc.2016.12.012.

Zhao, M., Gerritsma, M., Al Kobaisi, M., Hajibeygi, H., 2025. Algebraic dynamic multilevel (ADM) method for CO2 storage in heterogeneous saline aquifers. J. Comput. Phys. 539, 114202. http://dx.doi.org/10.1016/j.jcp.2025.114202, URL https://www.sciencedirect.com/science/article/pii/S0021999125004851.